European Journal of Pharmaceutical Sciences 200 (2024) 106840

Contents lists available at ScienceDirect

European Journal of Pharmaceutical Sciences

journal homepage: www.elsevier.com/locate/ejps

Advanced interpenetrating polymer networks for innovative gastroretentive formulations targeting *Helicobacter pylori* gastric colonization

Roberto Grosso [a], Elena Benito [a,*], Ana I. Carbajo-Gordillo [a], Manuel Jesús Díaz [b], M. Gracia García-Martín [a], M.-Violante de-Paz [a,*]

[a] *Departamento de Química Orgánica y Farmacéutica, Facultad de Farmacia, Universidad de Sevilla, C/ Prof. García González, n. 2, 41012, Seville, Spain*
[b] *PRO2TECS. ETSI, Universidad de Huelva, 21071, Huelva, Spain*

ARTICLE INFO

Keywords:
Semi-IPN
Guar gum
Superporous matrix
Helicobacter pylori
Gastric cancer
Mucoadhesive polymers
Amoxicillin
Vonoprazan
Korsmeyer-Peppas model

ABSTRACT

The escalating challenges of *Helicobacter pylori*-induced gastric complications, driven by rising antibiotic resistance and persistent cancer risks, underscore the demand for innovative therapeutic strategies. This study addresses this urgency through the development of tailored semi-interpenetrating polymer networks (semi-IPN) serving as gastroretentive matrices for amoxicillin (AMOX). They are biodegradable, absorb significant volume of simulated gastric fluid (swelling index > 360 %) and exhibit superporous microstructures, remarkable mucoadhesion, and buoyancy. The investigation includes assessment at pH 1.2 for comparative analysis with prior studies and, notably, at pH 5.0, reflecting the acidic environment in *H. pylori*-infected stomachs. The semi-IPN demonstrated gel-like structures, maintaining integrity throughout the 24-hour controlled release study, and disintegrating upon completing their intended function. Evaluated in gastroretentive drug delivery system performance, AMOX release at pH 1.2 and pH 5.0 over 24 h (10 %-100 %) employed experimental design methodology, elucidating dominant release mechanisms. Their mucoadhesive, buoyant, three-dimensional scaffold stability, and gastric biodegradability make them ideal for accommodating substantial AMOX quantities. Furthermore, exploring the inclusion of the potassium-competitive acid blocker (P-CAB) vonoprazan (VONO) in AMOX-loaded formulations shows promise for precise and effective drug delivery. This innovative approach has the potential to combat *H. pylori* infections, thereby preventing the gastric cancer induced by this pathogen.

1. Introduction

The American Cancer Society's estimates for stomach cancer (also known as gastric cancer) in the United States for 2023 are about 26,500 new cases (Society, 2023). These statistics position stomach neoplasms with higher incidence than larynx, ovary, or esophagus cancer within the studied population (Society, 2023). *Helicobacter pylori* (*H. pylori*) infection is recognized as the most significant risk factor for gastric cancer, emphasizing the importance of preventive measures (Fernández-Navarro et al., 2021). The presence of a stomach ulcer may indicate an ongoing colonization of the gastric mucosa by *H. pylori*, thus raising the risk of oncological transformation in the patient's cells (Hansson et al., 1996).

Currently, antibiotic-based therapies against this pathogen are far from foolproof, especially considering the dramatic increase in antibiotic-resistant *H. pylori* strains. Typical treatment regimens often involve the use of up to four drugs, including two or three antibiotics, with the aim of eradicating the pathogen, despite the uncertainty of their susceptibility (Grosso and De-Paz, 2022). While these complex therapeutic approaches aim to improve eradication rates, there are some key issues regarding the patient and the overall management of the disease (Yang et al., 2014; Malfertheiner et al., 2017): first, the frequent dosing requirements in combination therapies can negatively impact patient adherence; second, the presence of unnecessary antibiotics in combination therapies contributes to the development of broader antimicrobial resistance, further compromising the effectiveness of these treatments resulting in the inability to successfully eradicate the bacterium in at least 20 % of treated patients (Lee et al., 2022).

To minimize the emergence of new resistant strains, selecting the appropriate antibiotic is a must. The most common approach to combat

* Corresponding author at: Universidad de Sevilla, Departamento de Química Orgánica y Farmacéutica.
E-mail addresses: ebenito@us.es (E. Benito), vdepaz@us.es (M.-V. de-Paz).

https://doi.org/10.1016/j.ejps.2024.106840
Received 7 February 2024; Received in revised form 25 April 2024; Accepted 20 June 2024
Available online 21 June 2024

H. pylori infection is susceptibility-based therapy, wherein specific antibiotics are prescribed based on known sensitivity after testing the infecting strain (Goderska et al., 2018). This type of prescription, known as "triple therapy," typically involves one proton pump inhibitor (PPI) and two antibiotics, commonly clarithromycin along with either amoxicillin, levofloxacin, or metronidazole (Yang et al., 2014; Lee et al., 2022; Goderska et al., 2018; Guevara and Cogdill, 2020). Among the antibiotics examined, amoxicillin (AMOX) appears to have the lowest prevalence of resistance among *H. pylori* strains (except in Africa), making it a favorable candidate for an optimized dual therapeutic approach (AMOX and a PPI) to be studied as a first-line treatment for infections in most countries (Grosso and De-Paz, 2022). This is the reason why AMOX has been the antibiotic chosen for the present work. Its effectiveness is determined by the period when its concentration surpasses the established minimal inhibitory concentration (MIC) for *H. pylori,* rather than achieving higher drug levels (Yang et al., 2014; Scott et al., 2016).

In general terms, to maintain consistent active pharmaceutical ingredient (API) levels above the MIC for an extended period, frequent administration of the drug is typical. Additionally, reducing antibiotic doses and improving dosage pathways through decreased administration frequency, while ensuring antibiotic concentrations remain above the MIC, is crucial in managing these types of infections. Reduced dosing can be achieved by employing gastroretentive drug delivery systems (GRDDS), which may prolong retention in the stomach compared to conventional formulations, while ensuring controlled and sustained release of the API over time. Among the gastroretentive systems that have shown the greatest efficacy are: (a) floating drug delivery systems, that are designed to remain in the stomach for a prolonged period, avoiding rapid gastric transit and (b) mucoadhesive drug delivery systems, that can adhere to the stomach wall, enabling gradual release of the API until the system disintegrates. Both approaches serve the crucial function of ensuring prolonged gastric retention and controlled release of the drug (Tripathi et al., 2019), ultimately contributing to improved therapeutic outcomes.

To date, only a limited number of instances have been documented regarding the application of GRDDS for the treatment of *H. pylori* infections utilizing AMOX-loaded GRDDS. The most effective cases have been those characterized by floating and/or mucoadhesive properties (Grosso and De-Paz, 2022). In broad terms, achieving the desired floating behavior of a dosage form typically involves the inclusion of swelling enhancers or wicking agents (Chavanpatil et al., 2006), as well as the use of effervescent combinations (Tadros, 2010). Alternatively, floatability in AMOX-based formulations can be achieved through the incorporation of low-density lipids like sunflower oil (Dey et al., 2016) or light mineral oil in oil-entrapped buoyant beads (Tripathi et al., 2012). However, current formulations for floating AMOX-loaded GRDDS rely on multiple additional excipients to ensure buoyancy during release, rather than inherent microstructural properties. This excipient-based approach is costly and environmentally impactful. Consequently, we propose the development of floating devices without added excipients, leveraging their porous structure to ensure buoyancy. Moreover, when targeting the eradication of *H. pylori* infection, the formulation of mucoadhesive GRDDS could offer significant advantages. These systems have the ability to adhere to the stomach wall, withstand gastrointestinal motility for extended periods (Zhao et al., 2014), thus enhancing the localized action of the drug within the infected area (Mandal et al., 2016). Polymers possessing high mucoadhesive strength are essential for the successful design of such dosage forms. Despite the excellent properties of guar gum (GG) in terms of mucoadhesion, biocompatibility, and degradability, it has not been utilized in AMOX-loaded GRDDS. Additionally, the presence of GG in metronidazole formulations has been shown to facilitate solvent transfer to the drug cargo, resulting in sustained drug release attributed to GG hydration and swelling (Amin et al., 2016). We explore herein the formation of GG-based superporous, mucoadhesive polymeric matrices with potential buoyant properties to load large quantities of AMOX.

On the other hand and in previous drug release studies on AMOX-loaded GRDDS, notably, they have been primarily conducted at pH 1.2, although this is not the pH encountered in the surrounding of *H. pylori*-infested stomach tissue (*ca.* pH 5.0) (Thombre and Gide, 2016). For example, despite effective control of AMOX release at pH 1.2 demonstrated by floating devices (Awasthi et al., 2012), this efficacy has not been validated at the pH 5.0. The predominant form of AMOX in gastric environments may diverge at different pH as recorded in Fig. 1 [AMOX pk_a (strongest basic): 7.22; AMOX pk_a (strongest acidic): 3.23, values obtained from www.drugbank.com]. At pH 1.2, which represents the fasting stomach conditions, AMOX exists predominantly in its cationic form (Fig. 1A). However, it is important to note that AMOX is often co-administered with proton pump inhibitors or acid blockers in clinical practice, resulting in stomach pH of *ca* 5.0. At such pH, AMOX is present predominantly in its zwitterionic form (Fig. 1B). This aspect should be an important consideration in the development of GRDDS for the treatment of *H. pylori* infections, as the release profile of AMOX can be significantly influenced by the surrounding gastric pH. The reason why these studies have not been conducted at pH 5.0 in previous research remains unclear. Moreover, any system under investigation for *H. pylori* treatment should be evaluated not only at pH 1.2 (for comparative purposes with previously published systems) but also at pH 5.0, the pH at which the antibiotic must be released. Our investigation aims to address this gap in the existing literature.

Achieving a sustained and controlled 24-hour release of AMOX at pH 5.0 in GRDDS remains an ongoing objective. Burst release (> 40 % in 1 h, pH 1.2) is frequently observed in floating gel systems (Patel et al., 2011) often attributed to their rapid disintegration. While an initial peak release may aid in achieving the MIC, it is imperative to regulate this parameter in the final formulation. Additionally, hollow modular tablets or imprinted devices designed to accommodate a non-gastroretentive drug tablet showed suboptimal drug retention, with up to 90 % cumulative drug release within 1.5 h (Charoenying et al., 2020; Rossi et al., 2016). This goal can potentially be realized through the preparation of semi-interpenetrating polymer networks (semi-IPN), known for their structure stability as well as their enhanced rheological properties (Sánchez-Cid et al., 2023; Grosso et al., 2023).

Another crucial factor to consider is the diversity of drug cargo within each system, influencing the final area under the curve (AUC) for AMOX and, consequently, the quantity of drug accessible in the stomach for its antibacterial efficacy. Despite the significance of this data, it is typically not explicitly addressed in research papers. Evaluating and determining the impact of this parameter in release trials is one of the objectives of this study. For the present study, the selection of loading values (AMOX percentages: 10 %, 25 % and 40 %; AMOX per beads: 5.6 mg, 16,7 mg and 33.3 mg, respectively) was based on two parameters: the MIC of AMOX and the global volume of liquid and food in the stomach per day (2.5 L, taking into account the frequent stomach replenishment). The minimum chosen AMOX loading value for the AMOX-loaded beads was selected to ensure a cargo at least 4 times the MIC of AMOX (0.5 μg/mL) (Rossi et al., 2016), thereby ensuring that even with cumulative drug release values as low as 25 % in beads with the minimum AMOX loading, they would still meet the MIC and thus be effective in the treatment against *H. pylori.* Additionally, kinetic studies provide supplementary information that enables the identification of the mechanism behind the release, whether it is governed by the swelling of the formulation, the diffusion of the drug within the matrix, a combination of both, or another mechanism. These inquiries aim to elucidate the delivery pathway, providing a better understanding of the underlying principles.

On a different aspect, GRDDSs often encounter certain limitations that must be addressed for optimal performance in pharmaceutical formulations. They may have a tendency to adhere together upon administration, posing a risk of bowel obstruction (Iglesias et al., 2020). Incorporating biodegradable components into the semi-IPN to be

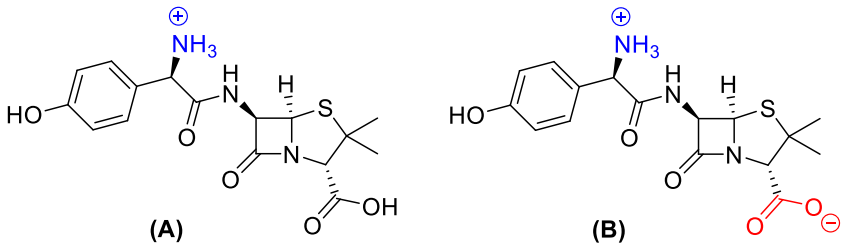

Fig. 1. Predominant forms of amoxicillin in gastric environments at (A) pH 1.2 and (B) pH 5.0.

utilized ensures their degradation in a 24-hour period (Grosso et al., 2023) enabling them to overcome such potential challenges. If the porous and floating characteristics of the semi-IPN are reduced due to the formation of intertwined crosslinked polymer chains, incorporating a mucoadhesive scaffold polymer, such as guar gum (GG), into semi-IPN matrices can ensure their prolonged retention in the stomach. This is achieved through interactions with mucin-epithelial surfaces, promoting adhesion to moist surfaces, including the stomach (Grosso and De-Paz, 2022).

As most antibiotics in anti-*H. pylori* therapies require an increase in intragastric pH for effective bactericidal action, the addition of a proton pump inhibitor to the combination is justified (Scott et al., 2016; Kiyotoki et al., 2020). Vonoprazan fumarate (VONO, also known as TAK-438) stands out as a novel potassium-competitive acid blocker (P-CAB) with distinct advantages over traditional proton pump inhibitors (Grosso and De-Paz, 2022). Although VONO does not possess direct antimicrobial activity against *H. pylori*, It offers sustained and robust inhibition of gastric acid secretion (Jenkins et al., 2015), quicker onset of action, longer plasma half-life (Kiyotoki et al., 2020; Mulford et al., 2022), and independence from genetic variability in metabolic enzymes (Sugano, 2018). Unlike proton pump inhibitors, VONO does not require a protective coating, can be taken with or without food, and maintains intragastric pH levels above 4 for over 24 h post-dose (Otake et al., 2016). The combination of AMOX and VONO presents a promising approach to combat *H. pylori* infections by addressing the limitations of traditional proton pump inhibitors, enhancing treatment efficacy, and potentially reducing antibiotic usage. AMOX's lower resistance development, coupled with VONO's ability to overcome proton pump inhibitor limitations, makes this regimen a compelling option for managing H. pylori infections.

The primary objective of this study is to determine the suitability of novel polymeric materials as gastroretentive matrices, possessing both enhanced rheological properties and high biodegradability, for prolonged retention in the stomach over a 24-hour period. The intended application is for the eradication of *H. pylori*, especially in patients at risk of developing gastric cancer. The materials for testing were prefabricated through the formation of semi-IPN. In this process, a polymeric material (Polymer 1) was synthesized *in situ* using an orthogonal and reliable polymerization method within the colloidal suspension of a second polymer: guar gum (GG). GG, a non-ionic, biocompatible, and naturally occurring polysaccharide with excellent mucoadhesive properties (Sharma et al., 2021; Casiraghi et al., 2020), serves as a temporary scaffold in IPN preparation. Its adhesiveness is crucial for potential use as gastroretentive drug delivery system (GRDDS) matrices, allowing adherence to the gastric mucosa and facilitating the achievement of the minimum inhibitory concentration (MIC) in affected areas. The study will assess various properties of the prepared polymeric materials, including swelling capacity, mucoadhesive properties, potential buoyancy, rheological properties, and porous structure. Additionally, their ability to encapsulate and control the release of the antibiotic AMOX. Kinetic release studies will investigate the impact of pH (pH 1.2 and pH 5.0), drug loading (from 10 % to 40 %), and the presence of biodegradable units in Polymer 1 (from 20 % to 80 %) on antibiotic release in simulated gastric environments. Furthermore, the study will explore the feasibility of co-administering AMOX-VONO in a single formulation, aiming for an AMOX-VONO dual approach for anti-H. pylori treatment.

2. Materials and methods

2.1. Chemicals

Chemicals used in this work were acquired from different suppliers and used as received. Guar gum (GG, product reference: G4129–250 G), diallyl carbonate (CAR), 2,2′-(ethylenedioxy)diethanethiol (EDDET), trimethylolpropane tris(3-mercaptopropionate) (TriT), methoxypol yethyleneglycol-350 (MeO-PEG-350), amoxicillin trihydrate (AMOX, Pharmaceutical Secondary Standard, 100 %) and type III pig mucin were acquired from Sigma-Aldrich (Madrid, Spain). Calcium chloride ($CaCl_2$) for the synthesis of acetaldehyde diallylacetal (monomer B) was provided by Fisher Scientific (part of Thermo Fisher Scientific; Massachusetts, USA). Alfa Aesar (part of Thermo Fisher Scientific; Massachusetts, USA) was the supplier of allyl alcohol. 2,2-Dimethoxy-2-phenylacetophenone (DMPA) and acetaldehyde were purchased from Acros Organics (part of Thermo Fisher Scientific; Massachusetts, USA) and agar-agar from Guinama, Barcelona, Spain. Vonoprazan fumarate was purchased from Ambeed (Illinois, USA).

2.2. Preparation of guar gum-based multicomponent hydrogels

Three systems were manufactured following the procedure outlined in a separate publication (Table 1) (Grosso et al., 2023). Monomer B (acetaldehyde diallylacetal) was synthesized beforehand, following the recipe described by Verdugo-Fernández (Verdugo-Fernández, 2020). The development of multicomponent hydrogels occurred through the growth of Polymer 1 within a colloidal suspension of Polymer 2 (GG) using a photoinitiated thiol-ene click reaction. For the formation of crosslinked Polymer 1, the allyl monomers employed were monomer CAR and the labile-under-acidic-conditions monomer B. EDDET was utilized as the dithiol and TriT served as the crosslinker (degree of crosslink: 8 %). The final concentration of the polymers was [Polymer 1] = [Polymer 2] = 4 % w/v, and the Polymer 1/Polymer 2 ratio was 1:1 (w/w) for all cases.

2.3. Characterization of guar gum-based semi-IPNs

The GG-based semi-IPN hydrogels employed in this study were comprehensively characterized in a prior investigation (Grosso et al., 2023). Subsequent research has focused on evaluating their swelling and floating properties, specifically for GG-p($B_{20}CAR_{80}$), GG-p($B_{50}CAR_{50}$) and GG-p($B_{80}CAR_{20}$). Floating lag time (FLT) and total floating time (FT) were determined by visual observation after dropping 50-mg beads of the lyophilized sample into a crystal vial containing saline solution 0.11 M (density equivalent to gastric fluids) (Asare-Addo et al., 2011). The temperature during the whole experiment was set to 37 °C, and the samples were left to float freely. The time required for the semi-IPN to rise to the surface and float was determined as floating lag time, while the total time for which the system remained buoyant before complete disintegration was recorded as total floating time.

Table 1
Preparation of guar-gum-based multicomponent hydrogels.

Multicomponent hydrogels	Polymer 1							Polymer 2
	Diallyl monomers			Dithiol	Xrlinker	Initiator	Global weight (mg)	GG (mg)
	B (μL)	CAR (μL)	Molar Ratio in the feed	EDDET (μL)	TriT (mg)	DMPA (mg)		
GG-p($B_{20}CAR_{80}$)	39.6	138.6	20:80	190.4	27	31	400	400
GG-p($B_{50}CAR_{50}$)	99.1	86.6	50:50	180.9	25.7	31	400	400
GG-p($B_{80}CAR_{20}$)	158.5	34.35	80:20	190.4	27	31	400	400

B: Acetaldehyde diallylacetal; CAR: diallyl carbonate; DMPA: 2,2-dimethoxy-2-phenylacetophenone; EDDET: 2,2′-(ethylenedioxy)diethanethiol, GG: guar gum; MeO-PEG 350: methoxypolyethyleneglycol-350; TriT: trimethylolpropane tris(3-mercaptopropionate); Xrlinker: crosslinker.
Reaction conditions: initiator = DMPA 10 %; MeO-PEG 350 = 1 g; distilled water added up to a final volume of 10 mL. T = 18 °C; UV radiation: 365 nm, 180 W, 10 min; reaction time: 24 h.

In vitro swelling experiments were conducted using 50-mg beads of lyophilized semi-IPN. The beads were placed into a crystal vial with 15 mL of distilled water. The temperature was set to 37 °C, and the samples were left to soak for 2 h. The weights of the swelled samples were measured (W_2) and compared to the original ones (W_1). The swelling index was interpreted as the number of times the system absorbed an amount of water equivalent to its weight (in percentage), and it was determined following Eq. (1):

$$Swelling\ index = (W_2 - W_1/W_1)\cdot 100 \quad (1)$$

Mucoadhesive properties were measured following the procedure recently employed by Villegas et al. (2021) and summarized next. Firstly, simulated mucosa was prepared by mixing 17 g of agar-agar with 700 mL of distilled water in a beaker, followed by heating the mixture to 95 °C for 15 min. After cooling to 70 °C, 2.5 g of type III pig mucin was added to the mixture and homogenized. Subsequently, before reaching room temperature, 30 mL of the mixture was poured into 6 cm diameter beakers and allowed to solidify at room temperature, resulting in the formation of the simulated mucosa. For the mucoadhesion assessment, beads of 50 mg of the IPN were placed on top of the simulated mucosa and allowed to rest for 2 min. The formulations were then covered with 60 mL of simulated gastric fluid (SGF) (Grosso et al., 2023) at pH 5.0. To simulate physiological conditions, the beakers were subjected to orbital agitation at 150 rpm and maintained at a temperature of 37 °C. The time required for each formulation to detach from the simulated gastric mucosa was measured, providing an indirect measurement of their mucoadhesive properties. The trials were conducted in triplicate and demonstrated statistical significance with $p < 0.05$ in each assay.

In the analysis of the multicomponent hydrogels prepared, both rheological measurements and images from field emission scanning electron microscope (SEM) were conducted/recorded at the CITIUS facilities of the Universidad de Sevilla. The rheological measurements of the hydrogels were performed in a Discovery HR-3 (TA Instruments, New Castle, DE, USA) rheometer, equipped with a Peltier temperature controller, at 25 °C, using a plate-plate geometry (diameter: 40 mm and 1 mm gap). Small-amplitude oscillatory shear (SAOS) tests from 0.12 to 62 rad s^{-1}, in the linear viscoelastic regime, were carried out. The linear viscoelasticity range was accomplished at a frequency of 1 Hz through strain amplitude sweeps. At least two replicates were done on fresh samples. Images were recorded specifically at the Microscopy Laboratories, by means of a field emission scanning electron microscope, Zeiss EVO, at an accelerating voltage of 10 kV using secondary electrons.

To perform the *in vitro* degradation studies of hydrogels, the methodology outlined by us for chitosan-based hydrogels was followed (Iglesias et al., 2020). Specifically, 40–60 mg dried beads (three samples per system) were placed in vials containing 10 mL of SGF (pH 5.0) and then incubated at 37 °C with shaking at 100 rpm. At various time points, the hydrogels were removed, rinsed with double-distilled water to eliminate any residual salinity, and weighed after ensuring that all surface water had been thoroughly blotted away. The residual mass of the hydrogels was calculated using Eq. (2), considering the initial weight of the samples.

$$\text{Residual mass } (\%) = W_t/W_0 \text{ x } 100 \quad (2)$$

where W_0 is the initial weight of the hydrogel and W_t is the weight of the hydrogel at each time point.

2.4. Calibration curves of amoxicillin and vonoprazan

Calibration curves of AMOX and VONO were obtained by UV spectrophotometric analyses of stock solutions of (a) AMOX at λ of 229 nm, and (b) VONO at λ of 207 nm, respectively. All the measurements were carried out in a UV-1280 Multipurpose UV–Visible Spectrophotometer (Shimadzu). The equations for the calibration curves for AMOX (Eq. (3)) and VONO (Eq. (4)) were found to be:

$$AMOX:\ y = 9084.2x + 0.0072\ \left(R^2 = 0.9994\right), \quad (3)$$

$$VONO:\ y = 35608x + 0.0369\left(R^2 = 0.9976\right), \quad (4)$$

where x corresponds to the concentration of drug (mmoles · mL^{-1}) and y to the detected absorbance.

2.5. Drug loading and experimental design methodology for in vitro drug release studies

Lyophilized samples from GG-p($B_{20}CAR_{80}$), GG-p($B_{50}CAR_{50}$) and GG-p($B_{80}CAR_{20}$) were chosen as matrices for sustained-released for AMOX. The beads (50 ± 5 mg) were prepared from freeze-dried hydrogels. The samples were weighed and placed in teflon cups, then stirred using an orbital stirrer (150 rpm, 25 °C, 3 h), resulting in beads with a diameter of 4.9 ± 0.5 mm. The systems were loaded with AMOX by addition of the drug [dissolved in dimethyl sulfoxide (DMSO); concentration: 500 mg · mL^{-1}] on the lyophilized IPN beads (50 mg) (Table 2).

Table 2
Samples for the experimental design methodology for *in vitro* drug release study.

Formulations for release studies	Semi-IPN used in the formulation	Drug loading (%)	Initial AMOX content (mg)
F1/F1'	GG-p($B_{20}CAR_{80}$)	40	33.33
F2/F2'	GG-p($B_{20}CAR_{80}$)	25	16.67
F3/F3'	GG-p($B_{20}CAR_{80}$)	10	5.56
F4/F4'	GG-p($B_{50}CAR_{50}$)	40	33.33
F5/F5'	GG-p($B_{50}CAR_{50}$)	25	16.67
F6/F6'	GG-p($B_{50}CAR_{50}$)	25	16.67
F7/F7'	GG-p($B_{50}CAR_{50}$)	10	5.56
F8/F8'	GG-p($B_{80}CAR_{20}$)	40	33.33
F9/F9'	GG-p($B_{80}CAR_{20}$)	25	16.67
F10/F10'	GG-p($B_{80}CAR_{20}$)	10	5.56

Release conditions: pH = 1.2 (F1 to F10); pH = 5.0 (F1' to F10'); T = 37 °C; lyophilized semi-IPN in each assay = 50-mg beads. AMOX: amoxicillin; IPN: interpenetrating polymer network.

To evaluate the effect of formulation composition on the *in vitro* drug release, a Box-Behnken experimental model design was utilized. Accordingly, ten AMOX-loaded semi-IPN-based formulations were prepared with drug loading percentages of 10 %, 25 %, or 40 % (in weight percentages) and the hydrogel types used were [GG-p($B_{20}CAR_{80}$), GG-p($B_{50}CAR_{50}$) or GG-p($B_{80}CAR_{20}$)] (Table 2).

For the dissolution studies, the cumulative drug release was monitored at 37 °C, at pH 1.2 and pH 5.0. Systems F5 and F6 were identical as required by the employed methodology. In the release assays at pH 1.2 and pH 5.0, the systems were distinguished and labeled as F1-F10 and F1′-F10′, respectively. Systems F5 and F6 (and F5'and F6') were intentionally kept identical in accordance with the methodology used. All the dissolution experiments were performed in triplicate, and statistical significance was observed with a p-value of less than 0.05 in each assay.

The drug-loaded materials were placed into dialysis tubes (1 kDa cut-off) and submerged in vessels containing either SGF-1.2 or SGF-5.0, depending on the sample. All the dissolution devices were subsequently place inside an orbital incubator at 37 °C and stirred gently (100 rpm) throughout the dissolution experiments. At each predetermined time interval, 5 mL of the medium were withdrawn from each vessel, and its absorbance was measured at 229 nm. Dilutions of the samples were conducted when necessary. An equal volume of prewarmed fresh medium was added to the dissolution vessels after each withdrawal. The amount of AMOX released by each system was calculated by means of the calibration curve (Eq. (3)).

Two additional release assays were conducted involving the incorporation of VONO into the formulations. In one scenario, VONO served as the sole drug, while in the other case, it was co-administered with the antibiotic AMOX. For the trials where VONO acted as the sole drug, the beads were prepared from the IPN GG p($B_{20}CAR_{80}$) using a procedure similar to the one described previously, with the exception that VONO was introduced into the Teflon cups and stirred along with the IPN (4 mg of VONO + 50 mg of IPN, 150 rpm, 25 °C, 3 h), resulting in a drug loading of 7.4 %. In the systems where AMOX and VONO were part of a dual-cargo formulation, VONO was added to the Teflon cups and stirred together with the IPN that had already been loaded with AMOX (4 mg of VONO + AMOX-loaded IPN), achieving a VONO loading of 7.4 % and AMOX loading of 10 %. The experimental parameters for the release assays corresponded to those outlined for assay F3 in Table 2. UV spectrophotometric measurements were taken at 207 and 229 nm at predetermined time intervals (Eqs. (3) and (4)).

To assess the influence of two independent variables from the semi-IPN (drug loading and percentage of monomer B) on the cumulative AMOX release after 8 h and 24 h (dependent variable), as well as the interactions among them, a Box-Behnken experimental design (CSS Statistica, StatSoft Inc., Tulsa, UK) was used. The number of experiments (*N)* necessary was defined by the following Eq. (5):

$$N = 2^k + 2{\cdot}k + cp \tag{5}$$

where k represents the number of factors (independent variables) involved in the study, and cp is the number of replicates of the central point (two in this case). Box-Behnken could be seen as a cube, consisting of a central point and the middle points of the edges. The total number of experiments required for each system, considering independent variables at three levels, was 10 (from F1 to F10 at pH 1.2, and from F1' to F10' at pH 5.0).

To facilitate direct comparison of the coefficients and visualization of the effects of each independent variable on the drug release, the values of the independent variables were normalized from −1 to +1 by using the Eq. (6):

$$X_n = \frac{X - \overline{X}}{(X_{max} - X_{min})/2} \tag{6}$$

where X_n is the normalized value of independent variables; X is the absolute experimental value of the variable concerned; $\overline{X}$ the mean of all fixed values for the variable in question; and X_{max} and X_{min} are the maximum and minimum values of the variable, respectively.

2.6. Kinetics modeling of drug release

Several kinds of kinetic models (zero-, first-order, and Higuchi) were applied to explain the drug release behaviors at both pH 1.2 and pH 5.0, and the model with the highest correlation coefficient (R^2) should be considered as the optimal fit. The release mechanism was also estimated according to the Korsmayer–Peppas kinetics model. The data were evaluated according to the following equations:

$$\text{Zero} - \text{ordermodel}: \; Q_t = Q_0 + k_0{\cdot}t \tag{7}$$

where Q_t is the amount of drug released at time t; Q_0 is the initial amount of drug in solution (zero in our case); k_0 is the zero order release constant.

$$\textit{First} - \textit{order model}: \; \log C = \log C_0 \; - \; k_1 t/2.303 \tag{8}$$

where C_0 is the initial concentration of drug; C is the drug concentration remaining at time t; k_1 is the first order release constant.

$$\textit{Higuchi model}: \; Q_t = k_H{\cdot}t^{1/2} \tag{9}$$

where Q_t is the amount of drug released at time t; k_H is the release rate constant for the Higuchi model.

$$\textit{Korsemeyer} - \textit{Peppas model}: \; M_t/M_\infty = \; k_{KP}{\cdot}t^n \tag{10}$$

where M_t/M_∞ is the fraction of drug released at time t; k_{KP} is the rate constant; n is the release exponent, indicative of the mechanism of drug release. First 60 % drug release data was fitted in Higuchi and Korsmeyer–Peppas model.

3. Results and discussion

In this research, we have successfully developed and presented ten gastroretentive AMOX formulations, leveraging the use of three innovative polymer matrices. These matrices were meticulously designed to possess the optimal attributes necessary for highly efficient gastroretentive applications, surpassing the limitations of previous systems (Grosso and De-Paz, 2022). Through our exploration of AMOX formulations utilizing these matrices, we have laid the foundation for the future development of simpler and more effective strategies in combating this widespread infection. Our significant achievement lies in the discovery of a straightforward and remarkably efficient method for delivering antibiotics, with a specific focus on AMOX, renowned for its exceptional effectiveness and minimal resistance issues observed across diverse regions of the world.

3.1. Preparation of guar gum-based multicomponent hydrogels

Crosslinked Polymer 1 (a biodegradable polycarbonate) was successfully synthesized using a thiol-ene click reaction that took place within a colloidal solution of GG (Polymer 2), a polysaccharide renowned for its excellent mucoadhesive properties (Sharma et al., 2021; Casiraghi et al., 2020) (Fig. 2). In this instance, Polymer 1 was synthesized through a photo-initiated process by reacting diallyl monomers (monomer CAR and monomer B) at different B:CAR ratios (20:80, 50:50, and 80:20) with the dithiol EDDET, and crosslinked using an 8 % molar ratio of TriT (Table 1). The three multicomponent hydrogels formed were designated based on the ratios of diallyl monomers utilized, namely, GG-p($B_{20}CAR_{80}$), GG-p($B_{50}CAR_{50}$), and GG-p($B_{80}CAR_{20}$). This atom-economical polymerization process occurred in a single step and was previously validated in IPN formation studies, demonstrating its robustness (Sánchez-Cid et al., 2023; Grosso et al.,

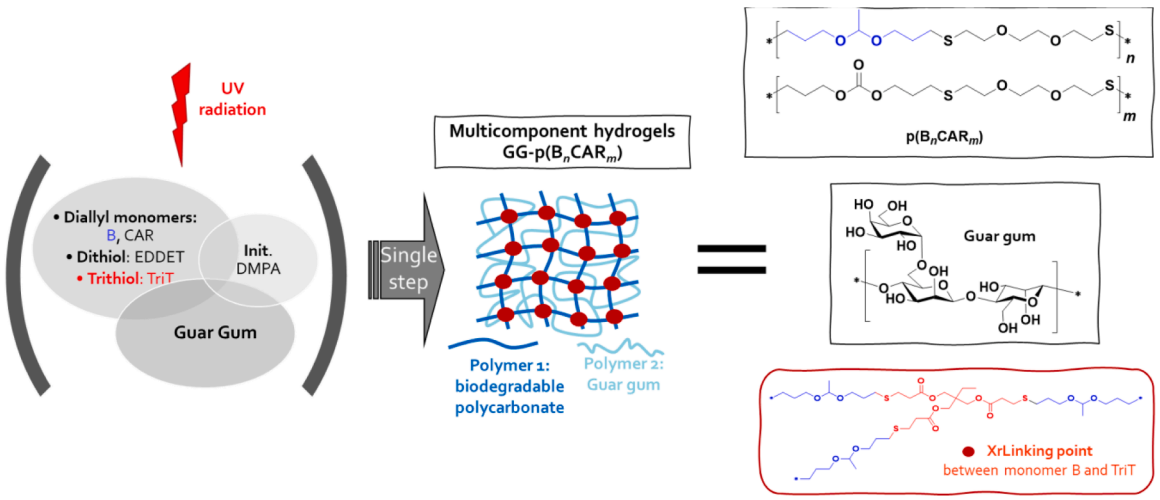

Fig. 2. Scheme for GG-based semi-IPN preparation. A unified approach for single-step multicomponent hydrogel synthesis by click chemistry.

2023). The synthetic method's reliability was confirmed by ^{1}H NMR, regardless of the diallyl monomers ratio used (Grosso et al., 2023). NMR analyses, which enable quantitative composition determination, revealed that materials compositions closely matched the feed (± 2.5 percentage points) for various diallyl monomer ratios (monomer CAR and monomer B). This finding indicates the reproducibility of the IPN preparation method.

The utilization of guar gum at a 4 % concentration in the formation of IPN is grounded in its polysaccharide nature, enabling hydrogel formation within this specific range (3.79 % to 4 %). This concentration is particularly suited for RAFT systems where a high gel consistency is not a prerequisite (Kamsali et al., 2020). Furthermore, our investigation has revealed that maintaining a Polymer 1:Polymer 2 ratio of 1:1 is optimal for IPN formation, especially when chitosan serves as Polymer 2. This ratio choice, validated against alternative ratios (2:1, 1:1, and 1:2), has been shown to enhance the efficacy of IPN formation in this polymer combination, underscoring its significance in the development of advanced materials for various applications (Sánchez-Cid et al., 2023).

As a result, the formation of stable and homogeneous three-dimensional networks that maintain their consistency over an extended period under bench conditions, was achieved. This behavior stands in stark contrast to the colloidal suspensions of GG alone, which rapidly disintegrate within a few hours, forming highly heterogeneous biphasic systems lacking gel-like consistency. All of it makes the final structure of the product to resemble a 3D network which may be capable of accommodating a drug.

3.2. Characterization of guar gum-based semi-IPN hydrogels

For the preparation of semi-IPN hydrogels as matrices in GRDDS, the biopolymer used in all the trials was GG due to its outstanding properties mentioned above. In this way, the generation of semi-IPNs resulted in more stable systems without chemically modifying GG, so its mucoadhesive and biodegradable properties could stay untouched. Interestingly, the proven biodegradability of Polymer 1 under stomach-like environmental conditions, precisely where *H. pylori* resides, emerges as another crucial aspect (Grosso et al., 2023). Such biodegradability is imparted by the presence of acid-sensitive acetal groups (from monomer B) within its structure (Grosso et al., 2023). This characteristic is particularly interesting for gastroretentive formulations based on these multicomponent hydrogels as it ensures the matrices' resilience to gastric motility while also guaranteeing their degradation once their use as a drug carrier for active pharmaceutical ingredients (APIs) ends, thereby preventing intestinal obstruction. Moreover, the evaluation of the influence that the percentage of these labile acetal groups in the IPNs (with different B:CAR ratios) in the drug release is one of our goals.

The IPNs are anticipated to exhibit nontoxic properties since the degradation of Polymer 1 results in the release of acetaldehyde and biocompatible oligomers. The latter are naturally eliminated through biological processes such as feces excretion. In terms of acetaldehyde production, a single bead (dosage form) generates minimal amounts, ranging from 0.68 mg to 2.73 mg. Therefore, these amounts can be considered negligible, constituting only a minute fraction of the total bead weight. On the other hand, acetaldehyde is a natural degradation product in the metabolism of ethanol in the human body, and it is rapidly metabolized to acetic acid within the organism. In addition to the aforementioned characteristics, various parameters were examined for each hydrogel, and the findings are documented below.

3.2.1. Rheological studies

The rheological analyses were conducted on the samples after a minimum waiting period of 48 h post-preparation to ensure the temporal stability of the hydrogels. This extended waiting period was necessary due to the fact that GG hydrogels, in contrast to semi-interpenetrating polymer network (semi IPN)-based hydrogels, exhibit a loss of gel structure within a period of less than 48 h. Therefore, to ensure accurate and consistent rheological measurements, a waiting period of 48 h was implemented for all semi-IPN. After preparation, rheological studies of the GG hydrogel were conducted immediately to capture its optimal rheological properties without any delay. It is worth noting that the semi IPN-based hydrogels demonstrated stability for a period of 6 months without significant alterations in their rheological parameters.

Table 3 provides the critical strain, plateau modulus, storage modulus, loss modulus, complex viscosity, and tangent delta values at a frequency of 1.00 rad/s for different semi-IPNs and the GG hydrogel as a blank. The experimental procedure commenced with strain sweep tests to identify the plateau region. The experimental data corresponding to the critical shear strain define the transition from linear to nonlinear viscoelastic behavior. It was noted that all the systems deviated from linearity beyond a strain of 0.388 %.

Subsequently, frequency sweep tests were performed, revealing the formation of strong gels in all the systems (Table 3, Fig. 3). Particularly noteworthy were the significantly higher values of elastic modulus (G') observed for the semi-IPN systems GG-p($B_{20}CAR_{80}$) and GG-p($B_{80}CAR_{20}$), where either the CAR monomer or the B monomer predominated in the feed. The multicomponent GG-p($B_{50}CAR_{50}$) system showcased a distinct frequency dependency, similar to the case when (*2R,3R*)-*N,N'*-diallyltartramide (TAR) was employed as the co-monomer in the same proportion [GG-p(TAR_{50} B_{50})] (Grosso et al., 2023). Across

Table 3
Critical strain, plateau modulus (G_N^o) storage modulus ($G_1^{'}$), loss modulus ($G_1^{''}$), complex viscosity (η_1^*) and tangent delta [tan (δ)] values at 1.00 rad/s for the different semi-IPNs evaluated and GG hydrogel as a blank.

Semi-IPN	Critical Strain (%)	G_N^o (Pa)	$G_1^{'}$(Pa)	$G_1^{''}$ (Pa)	η_1^* (Pa.s)	$tan\ (\delta)_1$
Blank GG	0.038 ± 0.004	454.1 ± 13.6	140.1 ± 4.21	91.1 ± 2.7	143.9 ± 4.3	0.65 ± 0.02
GG-p($B_{20}CAR_{80}$)	0.008 ± 0.001	3179.9 ± 65.4	2763.3 ± 82.3	590.9 ± 17.7	2837.6 ± 85.0	0.21 ± 0.01
GG-p($B_{50}CAR_{50}$)	0.073 ± 0.003	1028.0 ± 30.8	418.7 ± 12.6	202.0 ± 5.1	429.8 ± 10.9	0.48 ± 0.02
GG-p($B_{80}CAR_{20}$)	0.388 ± 0.013	5560.2 ± 121	4940.0 ± 128.2	1110.2 ± 23.3	5071.4 ± 132.1	0.22 ± 0.01

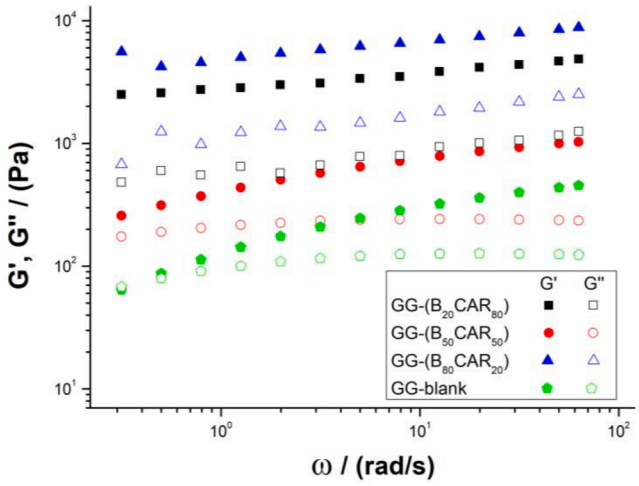

Fig. 3. Frequency sweep tests of the different systems evaluated: GG-p($B_{20}CAR_{80}$), GG-p($B_{50}CAR_{50}$), and GG-p($B_{80}CAR_{20}$) and guar gum as blank.

the frequency range, this system exhibited a steep slope, with G' values at high frequencies nearly one order of magnitude greater than loss modulus (G'') values. This behavior indicated an enhanced solid-like response with increasing frequency. "The plateau modulus, G_N^0, was determined as the G' value at the frequency where the loss tangent (tan δ) reaches its minimum (Liu et al., 2006). This modulus can be considered a measure of the degree of aggregation of the dispersed structural units or the density of physical entanglements, and therefore, it is related to the strength of the microstructural network (Baumgaertel and Winter, 1992). Notably, the rheological properties of the prepared systems were significantly influenced by their composition.

In essence, the entanglement between the polymer chains of Polymer 1 and Polymer 2 (GG) plays a crucial role in the rheological properties of the final products, ensuring the long-term stability of the three-dimensional scaffold for months under bench conditions while remaining biodegradable when submerged in simulated gastric fluids.

3.2.2. Microstructure, floating, swelling and mucoadhesive properties of multicomponent hydrogels

The examination of IPN buoyancy, swelling, and mucoadhesive properties (Table 4) showcased their significant potential as matrices in GRDDS. Swelling studies play a crucial role in understanding the drug release dynamics in GRDDSs (Amin et al., 2016). The swelling behavior of the matrices can significantly influence the release kinetics of encapsulated drugs, as biological fluids must enter the multiporous systems for drug dissolution testing. The release mechanisms can be driven by Fickian diffusion, erosion, swelling, or a combination of these processes. For example, the presence of GG in metronidazole formulations has been shown to facilitate solvent transfer to the drug cargo, resulting in sustained drug release attributed to GG hydration and swelling (Amin et al., 2016). This highlights the importance of understanding the impact of matrix composition on drug release kinetics. Furthermore, non-Fickian release is characterized by a high diffusion exponent value, while anomalous diffusion indicates a coupling of diffusion and erosion mechanisms, suggesting that the drug release is controlled by more than one process (Siepmann and Peppas, 2012). Thus, as water ingresses from the outer side to the bead core, the outer gel layer starts to erode, leading to a progressive decrease in volume and reduction in formulation weight (Ranade et al., 2012). The prepared matrices demonstrated significant swelling capacities (Table 4), which undoubtedly will have a significant impact on the release kinetics of encapsulated AMOX when employed in GRDDSs (Brannon-Peppas et al., 1990). On the other hand, the microstructural analysis of the prepared systems indicated superporous architectures, as depicted in SEM images (Fig. 4), contributing to the observed swelling behavior. This characteristic is attributed to interconnected pores facilitating water penetration into the 3D network, resulting in capillary-driven swelling (Bardonnet et al., 2006).

Stability studies of the multicomponent hydrogels in SGF at pH 5.0 were conducted to understand their behavior as matrices in GRDDS, measuring the mass of IPN at predetermined intervals after immersion in SGF at 37 °C (Fig. 5). The beads swelled, absorbing significant amounts of the fluid medium, followed by a phase of mass loss due to polymer disentanglement and erosion. As it will be assessed in Section 3.4, these processes, along with drug diffusion gradients, govern the release kinetics observed in 14 out of the 20 AMOX release assays (Anomalous/non-Fickian diffusion), with complete degradation within 48 h in all cases.

Furthermore, two out of the three semi-IPN prepared [GG-p($B_{50}CAR_{50}$) and GG-p($B_{80}CAR_{20}$)] displayed floating properties (Table 4). The development of buoyant systems represents a key strategy to attain successful GRDDSs (Iglesias et al., 2020). Various types of

Table 4
Swelling, floating and mucoadhesive studies of the multicomponent hydrogels.

Semi-IPN	Floating lag time (min)	Floating time (min)	Swelling index[a] (%)	Mucoadhesion[b] (h)
GG-p($B_{20}CAR_{80}$)	—	0	435 ± 48	38 ± 0.3
GG-p($B_{50}CAR_{50}$)	18 ± 2	>720	368 ± 35	30 ± 0.4
GG-p($B_{80}CAR_{20}$)	0	240 ± 10	434 ± 40	30 ± 0.2

[a] Swelling indexes represent the number of times the system absorbed an amount of water equivalent to its weight (in percentage). [b]Mucoadhesion tests measure the period the beads keep adhere to artificial gastric mucosa.

Floating assay conditions: mass of IPN beads = 50 mg; floating solution: saline solution 0.11 M; T: 37 °C.

Swelling assay conditions: mass of IPN beads = 50 mg; swelling solution: distilled water; T = 37 °C; soaking time = 2 h.

Mucoadhesive assay conditions: mass of IPN beads = 50 mg; adherent surface: artificial gastric mucosa; liquid medium: simulated gastric fluid; pH: 5.0; agitation: 150 rpm; T = 37 °C.

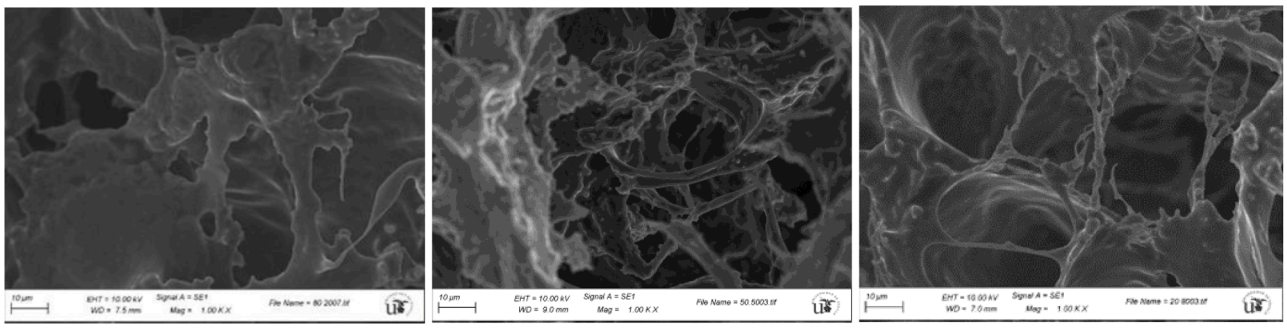

Fig. 4. SEM images from (a) GG-p($B_{20}CAR_{80}$); (b) GG-p($B_{50}CAR_{50}$); (c) GG-p($B_{80}CAR_{20}$).

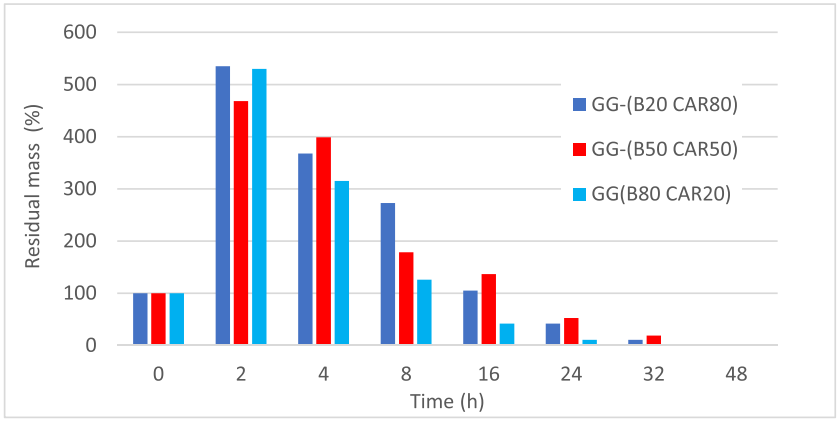

Fig. 5. *In vitro* degradation patterns of GG-based hydrogels conducted at pH 5.0 and 37 °C in SGF.

systems have been designed as AMOX-GRDDSs, ranging from floating beads (Rajinikanth and Mishra, 2009) to floating *in situ* gelling system (Patel et al., 2011; Rajinikanth et al., 2007), floating capsular devices obtained by 3D printing (Charoenying et al., 2020), bilayer floating tablets (Ranade et al., 2012), hollow tablets (Rossi et al., 2016), floating raft systems (Kamsali et al., 2020) or floating microballoons and/or spheres (Awasthi et al., 2012). In general terms, the formulations proposed for buoyant AMOX-loaded GRDDSs typically include two or three additional excipients to ensure buoyancy during the expected release period. However, the lack of examples where floatability is solely determined by the microstructure of the system suggests the need to address the costly and ecologically impactful excipient-containing approach in future GRDDS designs. The noteworthy aspect of the systems described in this study is that they exhibit inherent floating properties without the requirement of additional excipients and this characteristic represents a significant advancement compared to other formulations previously reported. Special attention should be thrown to GG-p($B_{50}CAR_{50}$) which was capable of floating for more than 12 h.

Additionally, in the quest to eliminate *H. pylori* infection, mucoadhesive dosage forms prove particularly advantageous for developing GRDDS. These forms can adhere to the stomach wall, prolong their retention in the gastrointestinal tract (Zhao et al., 2014), and thereby enhance the localized action of the drug in the infected area (Mandal et al., 2016). The development of dual-action formulations, specifically, floating and mucoadhesive systems for the treatment of *H. pylori* infections, represents an interesting approach to significantly prolong the gastric residence time of AMOX. A recent review on AMOX-loaded GRDDSs provides a few examples of such systems (Grosso and De-Paz, 2022). All prepared matrices exhibited outstanding mucoadhesive properties, remaining adhered to the mucosa for over 24 h, as indicated in Table 4. These exceptional mucoadhesive properties were attributed to the presence of GG in all compositions, a characteristic unaffected by the growth of Polymer 1 within its colloidal suspension.

In summary, the notable swelling, mucoadhesive and buoyant properties, coupled with their stable three-dimensional scaffold-like structures and biodegradability under gastric conditions, position these superporous hydrogels as potentially ideal matrices in gastroretentive formulations for drug encapsulation and release. This is particularly relevant for AMOX, the primary focus of the current study.

3.3. Drug loading and experimental design methodology for in vitro drug release studies

The current research primarily focuses on encapsulating the key antibiotic utilized for treating *H. pylori* infections, AMOX, within the developed polymeric matrices. To prevent an initial burst effect upon administering the formulation, the incorporation of the drug as a solid was discarded (Venkateswaramurthy et al., 2011). Instead, AMOX was loaded into the systems dissolved in DMSO, a nontoxic solvent at these concentrations (Galvao et al., 2014).

The impact of AMOX cargo and formulation composition on *in vitro* cumulative drug release (CDR) was evaluated using a Box-Behnken experimental model design, a response surface methodology (RSM) approach. Its significance lies in its ability to determine the most influential variables and any synergistic or antagonistic effects between them. By using the Box-Behnken design, we can determine the optimal conditions for drug release, ensuring that the drug is released at the right time and in the right amount, thereby improving the overall treatment outcome (Iglesias et al., 2020; Iglesias et al., 2018). The Box-Behnken experimental design is employed in this study to optimize AMOX concentration and allyl monomer ratio (CAR and B) in Polymer 1 formation. The AMOX concentration is chosen based on its minimum inhibitory

concentration (MIC) and frequent stomach replenishment, ensuring that even with CDR of 25 % in the lowest AMOX cargo, the MIC is met. The allyl monomer ratio is selected to ensure matrix degradability, influenced by monomer B concentration, impacting bead erosion, disintegration, and drug release profile. This approach enables determination of optimal conditions for drug release, enhancing treatment outcomes.

Ten AMOX-loaded semi-IPN-based formulations were prepared for this purpose (Table 2). These formulations involved different proportions of AMOX in the GRDDS, with final percentages fixed at 10 %, 25 %, or 40 % (w/w) (1st independent variable). Additionally, the IPN composition was varied by adjusting the molar percentage of the labile diallyl monomer (monomer B) in Polymer 1 (2nd independent variable). The ratios of monomer B, in mol percentages, were set at 20 %, 50 %, or 80 % [designated as p($B_{20}CAR_{80}$), GG-p($B_{50}CAR_{50}$) and GG-p($B_{80}CAR_{20}$), respectively]. As stated before, the different ratios of monomer B and monomer CAR in the hydrogels (Table 1) offer an intriguing aspect for investigating the CDR from the AMOX-loaded formulations. This is attributed to the variable biodegradability of the multicomponent hydrogels in the stomach, which has the potential to influence the release profile of AMOX.

In the proposed experimental design (Table 5), both independent and dependent variables have been normalized and correlated. Each property value in this study represents the average of three experimental results. The deviations of these parameters from their respective means were all found to be less than 5 %.

During the dissolution studies, the cumulative AMOX release was monitored at 37 °C, under pH conditions of 1.2 (SGF-1.2) and 5.0 (SGF-5.0). The selection of pH conditions in experimental investigations is a pivotal factor in assessing the effectiveness of therapeutic interventions. In this regard, dissolution studies were conducted at pH values representing the typical physiological range (pH 1.2) for comparative purposes with other systems, and at pH 5.0. It is a key aspect of the current work the decision to employ a pH of 5.0 in the research presented herein is grounded in the established necessity for an elevated intragastric pH milieu during anti-*H. pylori* treatment protocols, as mentioned above. In clinical practice, it is customary to co-administer proton pump inhibitors or potassium-competitive acid blockers alongside antibiotics to modulate gastric pH. Consequently, patients undergoing treatment for *H. pylori* infections frequently exhibit a less acidic gastric environment, (close to pH 5), in contrast to the lower pH levels observed in healthy individuals.

Table 5 displays the CDR values after 8 h and 24 h at pH 1.2 (F1-F10) and 5.0 (F1'-F10'). Remarkably, previously published AMOX release studies from floating devices were performed almost exclusively at pH 1.2. It is noteworthy that, although this is the pH of stomach under fasting conditions, it will not be the pH encountered in the surrounding of *H. pylori*-infested stomach tissue, which leads to higher pH figures than those found in healthy, empty stomachs (Thombre and Gide, 2016). Additionally, these values cannot be extrapolated for AMOX release at less acidic pH levels because the solubility of AMOX (Felix et al., 2016), and thus its release profile, is pH-dependent in gastric fluids. On the other hand, the decision to use the CDR figures after 8 h is based on its common usage as a reference time in other research studies (Tripathi et al., 2012; Amin et al., 2016; Awasthi et al., 2012; Ranade et al., 2012). However, it is also important to track the drug release for 24 h, as the objective of the present work is to achieve sustained and prolonged AMOX release in the stomach to effectively combat *H. pylori* infections. Moreover, another aspect to be taken into consideration is the diversity of drug cargo in each system, which ultimately influences the area under the curve (AUC) for AMOX and, consequently, the quantity of drug available in the stomach to exert its antibacterial action. Despite the significance of this information, it is often not explicitly included in research papers. In our case, this information is specifically incorporated (Tables 2 and 5). The amount of AMOX loaded into the formulations did not exceed 33.5 mg per 50 mg of polymer, which may seem significantly lower that the usually prescribed dose for AMOX (1 g/day (Villegas et al., 2021)), even when using 10 times the size of the sample. However, it must be highlighted that such amount of AMOX may not be needed

Table 5
Cumulative AMOX release at 8 h and at 24 h at pH 1.2 (F1-F10) and pH 5.0 (F1'-F10') from formulations with varying ratios of monomer B in multicomponent hydrogels and different initial AMOX cargo.

	Formulations	Multicomponent hydrogel used in the formulation	Monomer B in Polymer 1[a] (% mol)	AMOX conc. (%)	Monomer B in Polymer 1 (norm. values)	AMOX conc. (norm. values)	Cumulative AMOX release[b] (%)	
							at 8 h	at 24 h
pH 1.2	F1	GG-p($B_{20}CAR_{80}$)	20	10	-1	-1	65.18	98.45
	F2	GG-p($B_{20}CAR_{80}$)	20	25	-1	0	35.32	70.16
	F3	GG-p($B_{20}CAR_{80}$)	20	40	-1	1	24.87	45.52
	F4	GG-p($B_{50}CAR_{50}$)	50	10	0	-1	61.30	99.89
	F5	GG-p($B_{50}CAR_{50}$)	50	25	0	0	27.48	69.61
	F6	GG-p($B_{50}CAR_{50}$)	50	25	0	0	27.39	71.89
	F7	GG-p($B_{50}CAR_{50}$)	50	40	0	1	20.35	43.03
	F8	GG-p($B_{80}CAR_{20}$)	80	10	1	-1	72.72	91.90
	F9	GG-p($B_{80}CAR_{20}$)	80	25	1	0	30.49	63.49
	F10	GG-p($B_{80}CAR_{20}$)	80	40	1	1	17.18	34.66
pH 5.0	F1'	GG-p($B_{20}CAR_{80}$)	20	10	-1	-1	43.67	48.14
	F2'	GG-p($B_{20}CAR_{80}$)	20	25	-1	0	8.52	14.54
	F3'	GG-p($B_{20}CAR_{80}$)	20	40	-1	1	6.44	9.80
	F4'	GG-p($B_{50}CAR_{50}$)	50	10	0	-1	33.58	59.19
	F5'	GG-p($B_{50}CAR_{50}$)	50	25	0	0	12.78	21.69
	F6'	GG-p($B_{50}CAR_{50}$)	50	25	0	0	13.82	20.14
	F7'	GG-p($B_{50}CAR_{50}$)	50	40	0	1	11.39	26.91
	F8'	GG-p($B_{80}CAR_{20}$)	80	10	1	-1	26.33	41.12
	F9'	GG-p($B_{80}CAR_{20}$)	80	25	1	0	18.84	27.46
	F10'	GG-p($B_{80}CAR_{20}$)	80	40	1	1	13.08	21.44

[a]Molar ratio in percentage of monomer B in the feed related to total allylic monomers. [b]Each value is the average of three samples ($p < 0.05$).

when using these GRDDSs, as it was already stated in similar studies considering that the reported minimum inhibitory concentration (MIC) for AMOX in the stomach to eradicate *H. pylori* is around 0.5 μg/mL (Rossi et al., 2016). Specifically, the authors demonstrated that a dose of 200 mg of AMOX loaded into a sustained-release system could maintain concentrations in the stomach up to six fold higher than that corresponding to MIC for a prolonged time (Rossi et al., 2016). Therefore, if the evaluated polymeric systems were able to achieve a successful local delivery, doses as low as that (or even lower) could be loaded into them and effectively eradicate the pathogen.

The data obtained from the release assays at 8 h and 24 h (Table 5) were mathematically analyzed and a set of equations was derived and presented in Table 6. The analyses conducted at both time points have proven to be crucial for gaining a comprehensive understanding of the underlying dynamics that govern the drug release from these matrices and the findings will be discussed below.

Determining the independent variables that have the greatest and least influence on the dependent variable in the equations presented in Table 6 poses a challenge due to the inclusion of interactions between two independent variable terms. To address this complexity, Fig. 6 illustrates a graphical representation of the relationship between the studied variables. This figure provides a comparison of CDR at the two studied pH values, after 8 h (Fig. 6a) and 24 h (Fig. 6b).

The surface response of CDR at 8 h is depicted in Fig. 6a. In general, CDR values were higher at pH 1.2 compared to pH 5.0. This phenomenon can be attributed, in part, to the enhanced solubility of AMOX at pH 1.2, where it exists predominantly in its cationic form due to protonation of its ionizable groups. In contrast, at pH 5.0, AMOX primarily adopts its zwitterionic form, which is less soluble in an aqueous medium (AMOX acidic ionization constants: $pK_a\ R-COOH$: 2.90; $pK_a\ R-NH_3^+$: 7.40 (Felix et al., 2016). It is well-established that the release of drugs from polymeric matrices necessitates an initial dissolution step in the medium, allowing only the soluble fraction to diffuse from the formulation (Ahuja et al., 2007).

Remarkably, the most influential factor governing overall drug release seemed to be the initial AMOX cargo, as indicated by the pronounced slope of the represented surfaces concerning the initial AMOX concentration and the governing CDR equations (Table 6). In contrast, the content of monomer B regarding allyl monomers in the feed exerted a less significant influence in 8-hour studies.

Thus, at both pH, the minimum amounts of AMOX in the formulations (10 % by weight) resulted in the maximum release. Specifically, pH 1.2 exhibited the highest CDR values, particularly at low and medium AMOX levels, while similar figures were observed at both pH for high AMOX concentrations. The inverse relationship between initial drug cargo and CDR contradicts findings published by others (Venkateswaramurthy et al., 2011; Hadke and Khan, 2021), where higher drug concentrations result in greater release. One possible explanation for our results is that the interpenetrated structures can swell in gel-like systems, leading to improved mechanical properties but substantially reducing SGF circulation. Additionally, the presence of the drug in the pores of the gel matrix decreases the free volume available for SGF circulation, hindering the delivery of the dissolved drug by diffusion. Furthermore, in other systems, formulations with lower drug loading are analyzed, which may not saturate the system, ensuring free circulation of the aqueous medium (Venkateswaramurthy et al., 2011).

On the other hand, the evolution of CDR with changes in the content of monomer B regarding allyl monomers varied depending on the pH and the initial AMOX cargo. At pH 1.2, increasing the amount of monomer B in the polymer while keeping the AMOX cargo at its lowest resulted in higher values of cumulative drug release.

Furthermore, when the semi-IPN used had the highest monomer B content [GG-p($B_{80}CAR_{20}$)], the CDR at pH 1.2 significantly depended on the AMOX cargo. Hence, the highest values of CDR of all the experiments conducted at such pH were found at the highest levels of monomer B in the polymer and lowest levels of AMOX. Conversely, the lowest CDR values of all the series were observed when the formulations constituted by such semi-IPN were loaded with the maximum AMOX cargo tested.

Intriguingly, Fig. 6b, that records the results for 24-h analyses, exhibits a distinct behavior when compared to the observations at 8 h. In general, and as expected, higher levels of cumulative amoxicillin release were achieved at 24 h for both pH values. At the 24-hour mark, and following the tendency found in 8-hour analyses, the values for cumulative amoxicillin release at pH 1.2 were significantly higher than those found at pH 5.0.

Conversely, the significant finding from the experiments at 24 h was that the relative impact of monomer B content on cumulative drug release (CDR) increased compared to AMOX cargo. Thus, at pH 1.2, the influence of the independent variable monomer B content outweighed that of amoxicillin concentration on CDR. This augmented effect of the variable B content can be attributed to the degradability of Polymer 1, a property that may contribute to the loosening of the polymeric matrices, consequently facilitating drug release (Iglesias et al., 2020).

Indeed, acetal hydrolysis is influenced by the pH of the medium, with more pronounced effects observed as the pH becomes more acidic. Previous research indicated that at pH 5.0 (Liu and Thayumanavan, 2017), approximately 60 % of molecules in a sample of a small acetal-derived compound (prepared from acetaldehyde) underwent hydrolysis of acetal groups within 5 h. When studying the degradability of the same type of acetals in polymeric structures, a reduction in the degradation pattern was observed (Grosso et al., 2023).Therefore, it was expected that the hydrolysis of Polymer 1 in the synthesized GRDDS matrices would require even more time to achieve similar degradation percentages at pH 5.0. Certainly, component B was not statistically significant in the 8-hour release studies, but it became statistically relevant when the system was submerged in SGF at both pH 1.2 and pH 5.0 for 24 h, although the relative influences of both independent variables were more comparable at pH 5.0.

3.4. Kinetic studies on AMOX release

The presented facts recorded above become evident when the release profiles over time are depicted at different pH conditions (pH 1.2, Fig. 7; pH 5.0, Fig. 8). At pH 1.2, it was observed that the range of release varied from 35 to 100 % within 24 h (Table 5); this variability in release percentages is particularly intriguing due to the diverse values observed. The percentage of released AMOX was clearly dependent on the initial AMOX loading (Fig. 7a-7c), with values differing to each other by more than 50 percentage points (values in the range from 52.93 to 57.24) at 24 h.

Table 6
Equations yielded for cumulative drug release (CDR) at 8 h and at 24 h as a function of the independent variables (normalized values) from the experimental design.

Equation	R^2	df	F
$CDR(pH1.2;8h) = 13.5978\cdot \text{AMOX}^2 - 22.9655\cdot \text{AMOX} - 3.8071\cdot \text{AMOX}\cdot B + 30.1691$	0.984	3.6	102.36
$CDR(pH5.0;8h) = 8.9249\cdot AMOX^2 - 12.1104\cdot AMOX + 5.9931\cdot AMOX\cdot B + 13.4900$	0.943	3.6	28.35
$CDR(pH1.2;24h) = -3.9899\cdot B^2 - 4.0111\cdot B - 28.0046\cdot AMOX + 71.3528$	0.993	3.6	727.77
$CDR(pH5.0;24h) = 16.7003\cdot A^2OX^2 - 15.0510\cdot AMOX + 4.6667\cdot AMOX\cdot B - 8.8499\cdot B^2 + 23.6313$	0.964	4.5	34.44

AMOX: initial cargo of amoxicillin in the formulations (normalized values); B: content of monomer B regarding allyl monomers (normalized values); CDR: cumulative drug release.

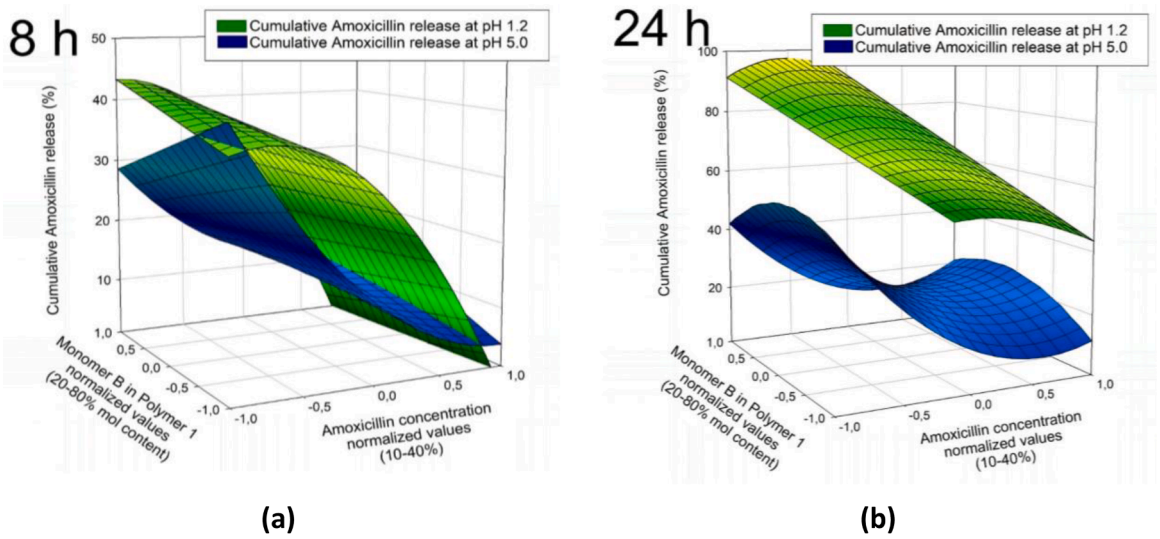

Fig. 6. Response surfaces for the cumulative release of amoxicillin at pH 1.2 and pH 5.0 after (a) 8 h and (b) 24 h.

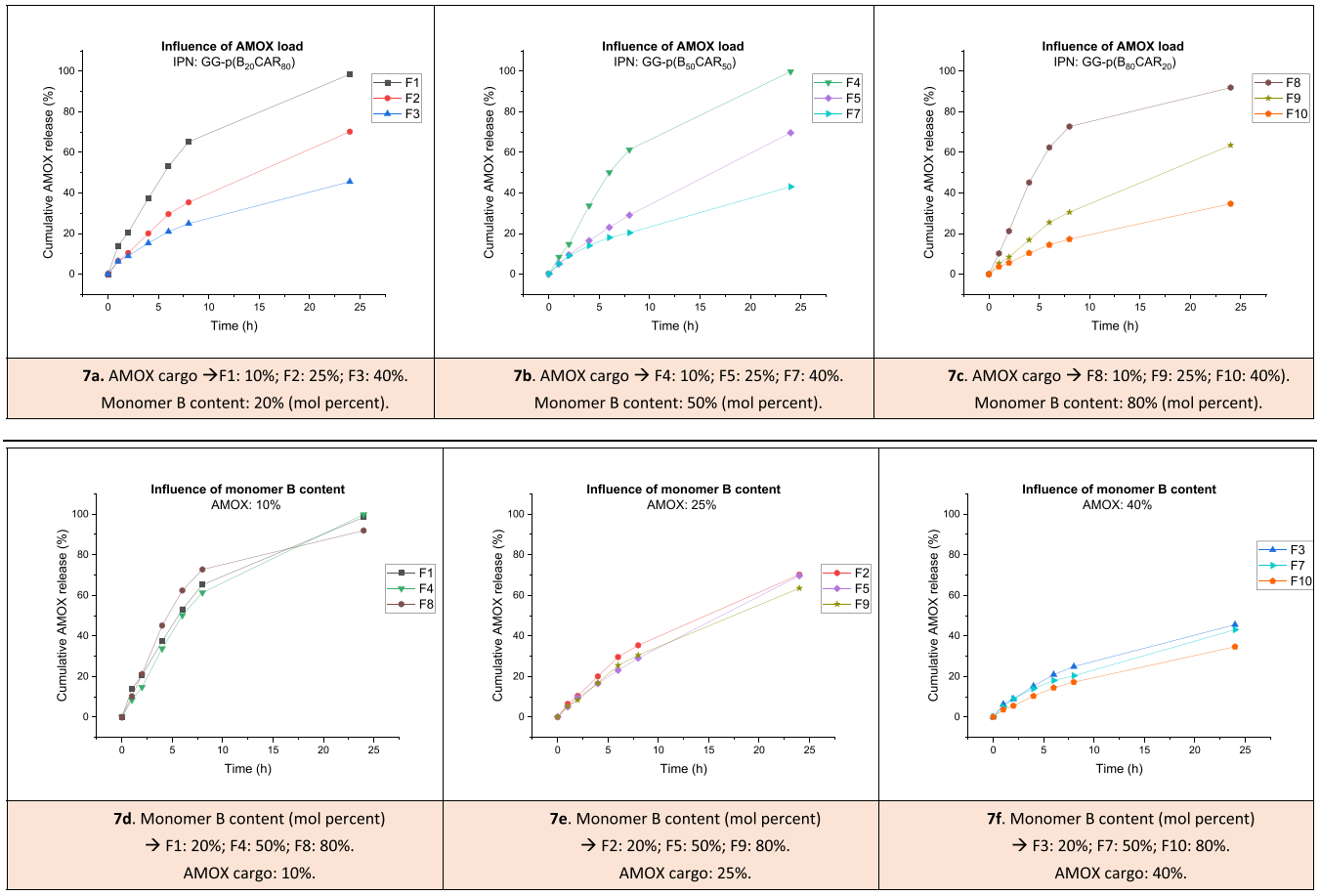

7a. AMOX cargo → F1: 10%; F2: 25%; F3: 40%. Monomer B content: 20% (mol percent).

7b. AMOX cargo → F4: 10%; F5: 25%; F7: 40%. Monomer B content: 50% (mol percent).

7c. AMOX cargo → F8: 10%; F9: 25%; F10: 40%). Monomer B content: 80% (mol percent).

7d. Monomer B content (mol percent) → F1: 20%; F4: 50%; F8: 80%. AMOX cargo: 10%.

7e. Monomer B content (mol percent) → F2: 20%; F5: 50%; F9: 80%. AMOX cargo: 25%.

7f. Monomer B content (mol percent) → F3: 20%; F7: 50%; F10: 80%. AMOX cargo: 40%.

Fig. 7. (1st part). Comparative plots of cumulative AMOX release (%) at pH 1.2 regarding monomer B content and initial AMOX cargo. **(2nd part).** Comparative plots of cumulative AMOX release (%) at pH 1.2 regarding monomer B content and initial AMOX cargo.

Additionally, a well-controlled AMOX release close to 100 % was achieved at pH 1.2 for the systems with an initial AMOX loading of 10 % (Fig. 7d). Moreover, the cumulative AMOX release showed minimal variation when transitioning from one semi-IPN to another (Fig. 7d-f).

In the release kinetics of AMOX conducted at pH 5.0, several significant findings emerged. Firstly, the cumulative AMOX release ranged from 10 to 59 % within 24 h (Table 5), with a notable decrease in CDR compared to pH 1.2 in all studied systems. This is in accordance with the findings from previous studies on mucoadhesive systems (Onuigbo et al., 2016; Moogooee et al., 2011). The release studies of AMOX conducted on floating GRDDSs are commonly examined at pH 1.2. Similarly, the release behavior of AMOX in mucoadhesive systems is primarily

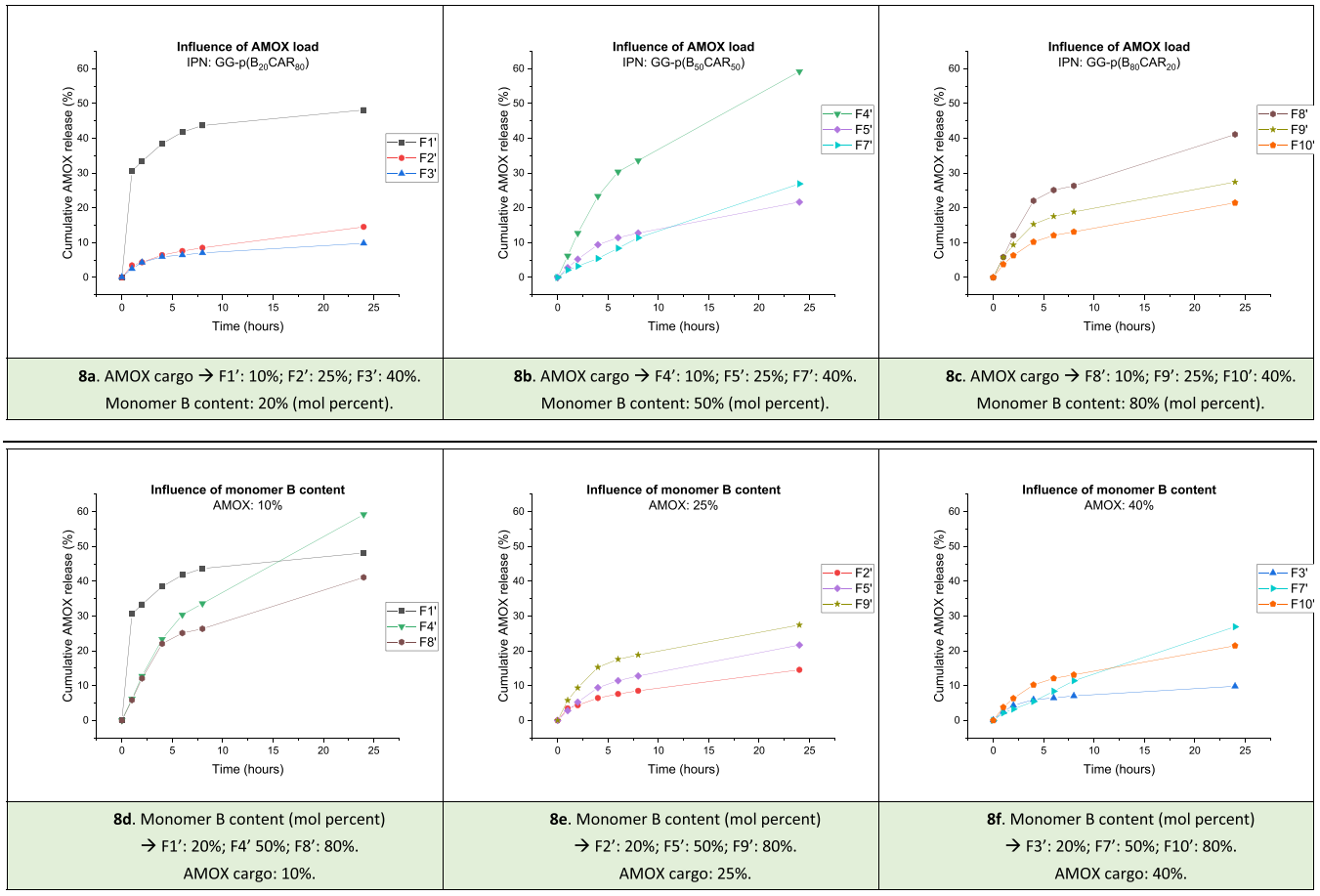

Fig. 8. (1st part). Comparative plots of cumulative AMOX release (%) at pH 5.0 regarding monomer B content and initial AMOX cargo.**(2nd part).** Comparative plots of cumulative AMOX release (%) at pH 5.0 regarding monomer B content and initial AMOX cargo.

investigated at pH 1.2. However, and in contrast to the floating systems, some studies in mucoadhesive formulations have also been carried out at pH 5.0 (Villegas et al., 2021) or pH *ca.* 7.0 (Onuigbo et al., 2016; Moogooee et al., 2011; Arif et al., 2021) (simulating gastric acid, gastric mucosa or optimal *H. pylori* survival conditions, respectively). The results indicated that *in vitro* AMOX release rates were higher at pH ≈1 compared to those observed at pH ≈7 (Onuigbo et al., 2016; Moogooee et al., 2011).

Secondly, as observed at pH 1.2, the CDR was more pronounced in formulations with lower initial AMOX loading, as evident in Figs. 8d-8f. Thirdly, the differences in drug release from formulations using the same semi-IPN and with an initial AMOX loading of 25 % and 40 % were not as marked (in some cases less than 10 percentage points) as those observed at pH 1.2. For instance, whereas at pH 1.2, F2/F3 (Fig. 7a) exhibited a difference of 24.64 percentage points in CDR, at pH 5.0, the corresponding drug release experiments (F2′/F3′, Fig. 8a) showed only a 4.74 percentage point difference.

Furthermore, it was corroborated that with the same semi-IPN (Fig. 8a-c), the differences in released AMOX also varied substantially depending on the initial AMOX loading, though not as prominently as at pH 1.2 (Fig. 7a-c). At pH 5.0, CDR varied within the range of 19.68 to 39.05 percentage points at 24 h when using the same multicomponent hydrogel.

At equal AMOX loading, the cumulative AMOX release plots exhibited more significant variation when transitioning from one system to another, in contrast to experiments conducted at pH 1.2 (compare Fig. 7d-f with the corresponding plots at pH 5.0 Fig. 8d-f). This behavior was previously noted in Box-Behnken studies and is attributed to the lower lability of acetal linkages at pH 5.0 compared to pH 1.2 and not to other factors such as GG-related effects. In contrast with ionic polymers, and as observed for other non-ionic polymers (Venkateswaramurthy et al., 2011), swelling of GG is not affected by pH variation. Therefore, a similar retardation effect on AMOX release due to GG is expected to occur at pH 1.2 and at pH 5.0 in GG-based formulations.

Subsequently, the *in vitro* release data were fitted into various release equations and kinetic models like zero-order, first-order, Higuchi equations and Korsmeyer–Peppas model (Singhvi and Singh, 2011). Regression coefficients (R^2) were determined to identify the most suitable model for describing the release kinetics. The results are presented in Table 7 for assays conducted at pH 1.2, and Table 8 for assays performed at pH 5.0. Among the various release kinetic models, the Korsmeyer-Peppas model exhibited the best fit for the *in vitro* dissolution data at pH 1.2, followed by the Higuchi model and first-order equation (Korsmeyer-Peppas > Higuchi model ≈ first order). For assays at pH 5.0, the Korsmeyer-Peppas model was also found to be the most suitable, followed by the Higuchi model (Korsmeyer–Peppas > Higuchi).

Remarkably, the Korsmeyer-Peppas model provided an excellent approximation of the release behavior of the systems, yielding R^2 values greater than 0.99 and 0.95 for all dissolution studies conducted at pH 1.2 and 5.0, respectively. In Eq. (10) of the Korsmeyer-Peppas model, the release exponent n indicates the mechanism of drug release. For the formulation under study, which involves spherical beads, Eq. (10) holds two distinct and physically realistic interpretations in these two special cases (Ritger and Peppas, 1987; Ritger and Peppas, 1987): (a) $n = 0.43$, indicating diffusion-controlled drug release (Fickian diffusion), and (b) $n = 0.85$, indicating swelling-controlled drug release (Case-II transport). Values of n between 0.43 and 0.85 suggest the superposition of both phenomena, signifying anomalous transport. At pH 1.2 (Table 7), a

Table 7
Mathematical modeling and release kinetics of amoxicillin for the prepared formulations (F1-F10) at pH 1.2.

Kinetic Model pH 1.2	Parameters	F1	F2	F3	F4	F5	F6	F7	F8	F9	F10
Zero-order	R^2	0.8594	0.9551	0.9318	0.8884	0.9915	0.9929	0.9580	0.7245	0.9656	0.9580
	k_0	3.8074	2.8108	1.7639	4.0122	2.8122	2.8900	1.6647	3.5414	2.5658	1.3746
First-order	R^2	0.9925	0.9986	0.9832	0.9713	0.9948	0.9911	0.9940	0.9511	0.9982	0.9870
	k_1	0.1787	0.0495	0.0230	0.2757	0.0050	0.0530	0.0214	0.1018	0.0415	0.0166
Higuchi	R^2	0.9570	0.9453	0.9751	0.9209	0.9601	0.9720	0.9861	0.9399	0.9218	0.9309
	k_H	23.3940	12.9380	8.9501	22.6380	10.0530	10.0170	7.4919	0.9399	10.9500	5.8484
Korsmeyer-Peppas	R^2	0.9929	0.9957	0.9932	0.9945	0.9975	0.9988	0.9909	0.9918	0.9940	0.9949
	n	0.7627	0.8449	0.6811	0.8630	0.8228	0.7430	0.6756	0.8696	0.8800	0.7727
	k_{KP}	13.1613	6.2044	5.9951	8.0947	5.1725	6.0007	5.9347	10.6586	4.9785	3.4938

R^2: regression coefficient; k_0: zero – order constant; k_1: first – order constant; k_H: Higuchi constant; k_{KP}: Korsmeyer – Peppas constant; n: diffusion coefficient

Table 8
Mathematical modeling and release kinetics of amoxicillin for the prepared formulations (F1'-F10') at pH 5.0.

Kinetic Model pH 5.0	Parameters	F1'	F2'	F3'	F4'	F5'	F6'	F7'	F8'	F9'	F10'
Zero-order	R^2	0.3812	0.8743	0.6867	0.8935	0.8744	0.7299	0.9915	0.7903	0.7601	0.8439
	k_0	1.2005	0.5192	0.311	2.2888	0.8206	0.6871	1.1003	1.5068	0.9662	0.7835
First-order	R^2	0.7587	0.9649	0.8474	0.9728	0.9256	0.8356	0.9979	0.8808	0.8576	0.9187
	k_1	0.0111	0.0051	0.0099	0.0343	0.0085	0.0067	0.0127	0.0180	0.0099	0.0081
Higuchi	R^2	0.8564	0.9959	0.9763	0.9646	0.9753	0.9702	0.9246	0.9596	0.9842	0.9868
	k_H	14.4260	3.0177	2.5525	12.8490	4.8350	5.2113	3.9180	10.3560	7.0961	4.9215
Korsmeyer-Peppas	R^2	0.992	0.992	0.950	0.983	0.983	0.952	0.985	0.952	0.963	0.982
	n	0.4274	0.4485	0.4868	0.8277	0.7414	0.5304	0.7989	0.7405	0.6105	0.6121
	k_{KP}	9.808	9.820	2.761	9.616	9.607	8.945	1.990	8.952	9.188	9.583

R^2: regression coefficient; k_0: zero – order constant; k_1: first – order constant; k_H: Higuchi constant; k_{KP}: Korsmeyer – Peppas constant; n: diffusion coefficient

release mechanism related to dynamic swelling (Case-II transport) was observed in 4 out of 10 samples, while the remaining 6 formulations exhibited anomalous transport, indicating the superposition of both phenomena, diffusion-controlled and swelling-controlled drug release. On the other hand, the analysis of the dissolution data obtained at pH 5.0 (Table 8) revealed diffusion-controlled drug release for the formulations in which the matrix was GG p($B_{20}CAR_{80}$) (F1', F2', and F3'). For the kinetics observed in the dissolution of AMOX from the other formulations, the trend leaned towards anomalous transport.

3.5. AMOX-VONO formulations. preeliminary studies

The favorable properties of the potassium-competitive acid blocker (P-CAB) VONO highlight the importance of investigating the AMOX-VONO combination and analyzing drug release mechanisms within the hydrogel matrix. Understanding the interaction between AMOX and VONO is crucial for ensuring improved efficacy comparable to traditional therapy, in eradicating *H. pylori* while reducing antibiotic misuse (Kiyotoki et al., 2020; Suzuki et al., 2020; Astruc et al., 2017). In such dual formulations, controlled release of AMOX is necessary, as is the complete delivery of VONO in the early stages following administration.

The feasibility of co-administering AMOX and VONO in a single multicomponent hydrogel-based formulation was investigated using the IPN GG-p($B_{20}CAR_{80}$). Initial trials revealed that, in formulations where only VONO was loaded in the IPNs, its release from the GG-based matrices (initial cargo: 4 mg, 7.4 % drug loading, sufficient for a single dose to raise stomach pH for 24-hour) was not fully achieved within an 8-hour period (VONO release: 44.33 %), and the required VONO concentration for a 24 h stomach pH increase was not met. This phenomenon may be due to the effective encapsulation of VONO within the three-dimensional network of the IPN. While these results are not ideal in this specific context, they could be of interest in the development of other GRDDS formulations using the designed IPN matrices.

However, when VONO (4 mg, 7.4 % drug loading) was loaded sequentially after AMOX (10 % drug loading), the former was completely released within 1.5 h, while the controlled release of AMOX was unaffected (at 8 hour period, cumulative AMOX release was 63.90 $\pm$ 1.32 %, very close to the figures achieved by the equivalent AMOX-loaded GRDDS: 65.18 $\pm$ 0.75 %). In such trials the matrix used was the same as in the previous experiments [GG-p($B_{20}CAR_{80}$)].

These drug delivery dynamics demonstrated that both drugs (AMOX and VONO) did not influence each other in their release profiles. This suggests that the initial addition of AMOX hindered the encapsulation of VONO within the IPN matrix, which keep it in the outer parts of the beads, leading to its first burst release and subsequently allowing the sustained release of AMOX. Furthermore, as previously stated, the Box-Behnken experimental design, a response surface methodology (RSM) approach, was employed to optimize the concentration of AMOX and the ratio of allyl monomers (CAR and B) in the formation of Polymer 1. This optimization ensures precise AMOX release timing and dosage, ultimately enhancing the overall treatment effectiveness.

4. Conclusions

In conclusion, this research has successfully developed ten innovative gastroretentive formulations loaded with AMOX, utilizing three distinct polymer matrices. These matrices were carefully designed to possess optimal attributes, surpassing limitations of previous systems,

and laying the groundwork for more efficient strategies in combating *H. pylori* infections. The novel matrices displayed superporous microstructures with exceptional mucoadhesive properties, buoyancy, and biodegradability in the gastric environment. Polymer 1, in conjunction with guar gum, provided a stable three-dimensional scaffold with prolonged drug release, while remaining biodegradable to prevent intestinal obstruction.

The formulations showed promising results, displaying a superporous architecture with significant swelling upon contact with biological fluids, and demonstrating prolonged drug release. Their performance as gastroretentive drug delivery systems for AMOX was assessed at different pH levels, providing valuable insights into their release kinetics and mechanisms. The Korsmeyer-Peppas model was found to best fit the *in vitro* dissolution data, indicating a combination of diffusion-controlled and swelling-controlled drug release.

Furthermore, the co-administration of VONO and AMOX within a single system was explored and the feasibility of incorporating both APIs into a unified formulation employing these multicomponent hydrogels was demonstrated. Importantly, the release profile of AMOX remained unaffected despite its presence alongside VONO in the formulation. In the upcoming phase of the research, the focus will shift towards investigating the toxicity of the formulations in various tissues to ensure their safety for clinical applications. Scaling up the production of these formulations to meet the requirements of preclinical and clinical studies will be a key objective as well as *in-vivo* trials to evaluate their effectiveness in combating *H. pylori infections*.

In summary, these advanced gastroretentive formulations hold significant promise for precise and effective drug delivery, with a specific focus on combating *H. pylori* infections and preventing gastric cancer. Their capacity to simultaneously administer VONO for rapid absorption and ensure controlled release of AMOX underscores their potential. These combined formulations mark a substantial advancement in the treatment of *H. pylori* infections, offering a combination of ideal properties and sustained release mechanisms. This innovation introduces novel opportunities for enhancing therapeutic strategies, ultimately benefiting individuals at risk of gastric cancer development.

Funding

This research was funded by MICIU/AEI/10.13039/501100011033, grant number PID2020-115916GB-I00.

CRediT authorship contribution statement

Roberto Grosso: Writing – original draft, Visualization, Validation, Methodology, Investigation, Conceptualization. **Elena Benito:** Writing – review & editing, Validation, Supervision, Resources, Project administration, Methodology, Investigation, Formal analysis, Data curation. **Ana I. Carbajo-Gordillo:** Visualization, Validation, Investigation, Formal analysis, Data curation. **Manuel Jesús Díaz:** Writing – original draft, Visualization, Validation, Investigation, Formal analysis, Data curation. **M. Gracia García-Martín:** Writing – review & editing, Supervision, Resources, Project administration, Methodology, Investigation, Formal analysis. **M.-Violante de-Paz:** Writing – review & editing, Writing – original draft, Visualization, Validation, Supervision, Resources, Project administration, Methodology, Investigation, Funding acquisition, Formal analysis, Data curation, Conceptualization.

Data availability

Data will be made available on request.

Acknowledgments

The authors want to acknowledge CITIUS for granting access to and their assistance with microscopy, NMR, functional characterization and biology services as well as El Fondo Europeo de Desarrollo Regional (FEDER), and La Consejería de Economía y Conocimiento (Junta de Andalucía), for support (Grant Number US-1380587).

References

Ahuja, N., Katare, O.P., Singh, B., 2007. Studies on dissolution enhancement and mathematical modeling of drug release of a poorly water-soluble drug using water-soluble carriers. Eur. J. Pharm. Biopharm. 65, 26–38. https://doi.org/10.1016/j.ejpb.2006.07.007.

Amin, M.L., Ahmed, T., Mannan, M.A., 2016. Development of floating-mucoadhesive microsphere for site specific release of metronidazole. Adv. Pharm. Bull. 6, 195–200. https://doi.org/10.15171/apb.2016.027.

Arif, M., Sharaf, M., Samreen, Q.Dong, Wang, L., Chi, Z., Liu, C.-G., 2021. Bacteria-targeting chitosan/carbon dots nanocomposite with membrane disruptive properties improve eradication rate of Helicobacter pylori. J. Biomater. Sci. 32, 2423–2447. https://doi.org/10.1080/09205063.2021.1972559. Polymer Edition.

Asare-Addo, K., Levina, M., Rajabi-Siahboomi, A.R., Nokhodchi, A., 2011. Effect of ionic strength and pH of dissolution media on theophylline release from hypromellose matrix tablets - Apparatus USP III, simulated fasted and fed conditions. Carbohydr. Polym. 86, 85–93. https://doi.org/10.1016/j.carbpol.2011.04.014.

Astruc, B., Jenkins, H., Jenkins, R., 2017. Effect of therapeutic and supratherapeutic doses of vonoprazan on the QT/QTc interval in a phase I randomized study in healthy subjects. Clin. Transl. Sci. 10, 208–216. https://doi.org/10.1111/cts.12452.

Awasthi, R., Kulkarni, G.T., Pawar, V.K., Garg, G., 2012. Optimization studies on gastroretentive floating system using response surface methodology. AAPS PharmSciTech. 13, 85–93. https://doi.org/10.1208/s12249-011-9730-y.

Bardonnet, P.L., Faivre, V., Pugh, W.J., Piffaretti, J.C., Falson, F., 2006. Gastroretentive dosage forms: overview and special case of Helicobacter pylori. J. Controll. Rel. 111, 1–18. https://doi.org/10.1016/j.jconrel.2005.10.031.

Baumgaertel, M., Winter, H.H., 1992. Interrelation between continious and discrete time spectra. J. Nonnewton. Fluid. Mech. 44, 15–36.

Brannon-Peppas, L., Peppas, N.A., Brannon-Peppas, L., 1990. The equilibrium swelling behavior of porous and non-porous hydrogels. In: Harland, R.S. (Ed.), Absorbent Polymer Technology. Elsevier, Amsterdam, pp. 67–102.

Casiraghi, A., Gennari, C.G., Musazzi, U.M., Ortenzi, M.A., Bordignon, S., Minghetti, P., 2020. Mucoadhesive budesonide formulation for the treatment of eosinophilic esophagitis. Pharmaceutics 12, 211–222. https://doi.org/10.3390/pharmaceutics12030211.

Charoenying, T., Patrojanasophon, P., Ngawhirunpat, T., Rojanarata, T., Akkaramongkolporn, P., Opanasopit, P., 2020. Fabrication of floating capsule-in-3D-printed devices as gastro-retentive delivery systems of amoxicillin. J. Drug Deliv. Sci. Technol. 55, 101393 https://doi.org/10.1016/j.jddst.2019.101393.

Chavanpatil, M.D., Jain, P., Chaudhari, S., Shear, R., Vavia, P.R., 2006. Novel sustained release, swellable and bioadhesive gastroretentive drug delivery system for ofloxacin. Int. J. Pharm. 316, 86–92. https://doi.org/10.1016/j.ijpharm.2006.02.038.

Dey, S.K., De, P.K., De, A., Ojha, S., De, R., Mukhopadhyay, A.K., Samanta, A., 2016. Floating mucoadhesive alginate beads of amoxicillin trihydrate: a facile approach for H. pylori eradication. Int. J. Biol. Macromol. 89, 622–631. https://doi.org/10.1016/J.IJBIOMAC.2016.05.027.

Felix, I.M.B., Moreira, L.C., Chiavone-Filho, O., Mattedi, S., 2016. Solubility measurements of amoxicillin in mixtures of water and ethanol from 283.15 to 298.15 K. Fluid Phase Equil. 422, 78–86. https://doi.org/10.1016/j.fluid.2016.02.040.

P. Fernández-Navarro, R. Roquette, O. Nuñez, M. de Sousa-Uva, J. García-Pérez, G. López-Abente, B. Nunes, M. González-Sánchez, J. Dinis, R. Carmona, J. Rocha Rodrigues, N. Aragonés, M. Bento, A. Castelló, R. Rego, V. Lope, R. Henrique, E. Boldo, A. Pais, N. Fernández de Larrea-Baz, J. Bastos, R. Ramis, B. Carrito, R. Pastor-Barriuso, A. Miranda, B. Pérez-Gómez, G. Forjaz, C. Matias Dias, M. Pollán, Atlas of cancer mortality in Portugal and Spain (2003-2012), 2021.

Galvao, J., Davis, B., Tilley, M., Normando, E., Duchen, M.R., Cordeiro, M.F., 2014. Unexpected low-dose toxicity of the universal solvent DMSO. FASEB J. 28, 1317–1330. https://doi.org/10.1096/fj.13-235440.

Goderska, K., Agudo Pena, S., Alarcon, T., 2018. Helicobacter pylori treatment: antibiotics or probiotics. Appl. Microbiol. Biotechnol. 102, 1–7. https://doi.org/10.1007/s00253-017-8535-7.

Grosso, R., Benito, E., Carbajo-Gordillo, A.I., García-Martín, M.G., Perez-Puyana, V., Sánchez-Cid, P., De-Paz, M.-V., 2023. Biodegradable guar-gum-based super-porous matrices for gastroretentive controlled drug release in the treatment of helicobacter pylori: a proof of concept. Int. J. Mol. Sci. 24, 1–23. https://doi.org/10.3390/ijms24032281, 2281.

Grosso, R., De-Paz, M.V., 2022. Scope and limitations of current antibiotic therapies against helicobacter pylori: reviewing amoxicillin gastroretentive formulations. Pharmaceutics 14, 1340. https://doi.org/10.3390/pharmaceutics14071340.
Guevara, B., Cogdill, A.G., 2020. Helicobacter pylori: a review of current diagnostic and management strategies. Dig. Dis. Sci. 65, 1917–1931. https://doi.org/10.1007/s10620-020-06193-7.
Hadke, J., Khan, S., 2021. Preparation of sterculia foetida-pullulan-based semi-interpenetrating polymer network gastroretentive microspheres of amoxicillin trihydrate and optimization by response surface methodology. Turk. J. Pharm. Sci. 18, 388–397. https://doi.org/10.4274/tjps.galenos.2020.33341.
Hansson, L.-E., Nyrén, O., Hsing, A.W., Bergström, R., Josefsson, S., Chow, W.-H., Fraumeni, J.F., Adami, H.-O., 1996. The risk of stomach cancer in patients with gastric or duodenal ulcer disease. N. Engl. J. Med. 335, 242–249. https://doi.org/10.1002/ijc.22123.
Iglesias, N., Galbis, E., Díaz-Blanco, M.J., de-Paz, M.V., Galbis, J.A., 2018. Loading studies of the anticancer drug camptothecin into dual stimuli-sensitive nanoparticles. Stability scrutiny. Int. J. Pharm. 550, 429–438. https://doi.org/10.1016/j.ijpharm.2018.08.026.
Iglesias, N., Galbis, E., Romero-Azogil, L., Benito, E., Lucas, R., García-Martín, M.G., De-Paz, M.-V., 2020a. In-depth study into polymeric materials in low-density gastroretentive formulations. Pharmaceutics 12, 1–49. https://doi.org/10.3390/pharmaceutics12070636, 636.
Iglesias, N., Galbis, E., Valencia, C., Díaz-Blanco, M.J., Lacroix, B., De-Paz, M.-V., 2020b. Biodegradable double cross-linked chitosan hydrogels for drug delivery: impact of chemistry on rheological and pharmacological performance. Int. J. Biol. Macromol. 165, 2205–2218. https://doi.org/10.1016/j.ijbiomac.2020.10.006.
Jenkins, H., Sakurai, Y., Nishimura, A., Okamoto, H., Hibberd, M., Jenkins, R., Yoneyama, T., Ashida, K., Ogama, Y., Warrington, S., 2015. Randomised clinical trial: safety, tolerability, pharmacokinetics and pharmacodynamics of repeated doses of TAK-438 (vonoprazan), a novel potassium-competitive acid blocker, in healthy male subjects. Alimentary Pharmacol. Therap. 41, 636–648. https://doi.org/10.1111/apt.13121.
Kamsali, A., Eranti, B., Ch, M., Manne, R., Barghav, G.C., Reddy, P.S., 2020. Development and optimization of amoxicillin floating raft system to effectively treat helicobacter pylori infection. ARS Pharm. 61, 163–168.
Kiyotoki, S., Nishikawa, J., Sakaida, I., 2020. Efficacy of vonoprazan for helicobacter pylori eradication. Internal Med. 59, 153–161. https://doi.org/10.2169/internalmedicine.2521-18.
Lee, Y.-C., Dore, M.P., Graham, D.Y., 2022. Diagnosis and treatment of helicobacter pylori infection. Chin. J. Gastroenterol. 73, 183–195. https://doi.org/10.31146/1682-8658-ecg-193-9-119-127.
Liu, B., Thayumanavan, S., 2017. Substituent effects on the pH sensitivity of acetals and ketals and their correlation with encapsulation stability in polymeric nanogels. J. Am. Chem. Soc. 139, 2306–2317. https://doi.org/10.1021/jacs.6b11181.
Liu, C., He, J., van Ruymbeke, E., Keunings, R., Bailly, C., 2006. Evaluation of different methods for the determination of the plateau modulus and the entanglement molecular weight. Polymer (Guildf.) 47, 4461–4479. https://doi.org/10.1016/j.polymer.2006.04.054.
Malfertheiner, P., Megraud, F., O'Morain, C., Gisbert, J.P., Kuipers, E.J., Axon, A., Bazzoli, F., Gasbarrini, A., Atherton, J., Graham, D.Y., Hunt, R., Moayyedi, P., Rokkas, T., Rugge, M., Selgrad, M., Suerbaum, S., Sugano, K., El-Omar, E., Agreus, L., Andersen, L.P., Coelho, L., Delchier, J.C., Di Mario, F., Dinis-Ribeiro, M., Fischbach, W., Flahou, B., Fock, K.M., Gasbarrini, G., Gensini, G., Goh, K.L., Herrero, R., Kupcinskas, L., Lanas, A., Leja, M., Machado, J.C., Mahachai, V., Milosavljevic, T., Niv, Y., Ristimaki, A., Tepes, B., Vaira, D., Vieth, M., You, W., 2017. Management of helicobacter pylori infection-the maastricht v/florence consensus report. Gut 66, 6–30. https://doi.org/10.1136/gutjnl-2016-312288.
Mandal, U.K., Chatterjee, B., Senjoti, F.G., 2016. Gastro-retentive drug delivery systems and their *in vivo* success: a recent update. Asian J. Pharm. Sci. II, 575–584. https://doi.org/10.1517/17425247.2011.584867.
Moogooee, M., Ramezanzadeh, H., Jasoori, S., Omidi, Y., Davaran, S., 2011. Synthesis and *in vitro* studies of cross-linked hydrogel nanoparticles containing amoxicillin. J. Pharm. Sci. 100, 1057–1066. https://doi.org/10.1002/jps.22351.
Mulford, D.J., Leifke, E., Hibberd, M., Howden, C.W., 2022. The effect of food on the pharmacokinetics of the potassium-competitive acid blocker vonoprazan. Clin. Pharmacol. Drug Dev. 11, 278–284. https://doi.org/10.1002/cpdd.1009.
Onuigbo, E., Onugwu, A., Nwocha, M., Odiase, A., Attama, A., 2016. Preparation and *in vitro* evaluation of amoxicillin encapsulated in alginate-coated chitosan microparticles. Trop. J. Pharm. Res. 15, 2303–2309. https://doi.org/10.4314/tjpr.v15i11.2.
Otake, K., Sakurai, Y., Nishida, H., Fukui, H., Tagawa, Y., Yamasaki, H., Karashima, M., Otsuka, K., Inatomi, N., 2016. Characteristics of the novel potassium-competitive acid blocker vonoprazan fumarate (TAK-438). Adv. Ther. 33, 1140–1157. https://doi.org/10.1007/s12325-016-0345-2.
Patel, D.M., Patel, D.K., Patel, C.N., 2011. Formulation and evaluation of floating oral in situ gelling system of amoxicillin. ISRN Pharm. 2011, 1–8. https://doi.org/10.5402/2011/276250.
Rajinikanth, P.S., Balasubramaniam, J., Mishra, B., 2007. Development and evaluation of a novel floating *in situ* gelling system of amoxicillin for eradication of Helicobacter pylori. Int. J. Pharm. 335, 114–122. https://doi.org/10.1016/J.IJPHARM.2006.11.008.
Rajinikanth, P.S., Mishra, B., 2009. Stomach-site specific drug delivery system of clarithromycin for eradication of Helicobacter pylori. Chem. Pharm. Bull. 57, 1068–1075. https://doi.org/10.1248/cpb.57.1068.
Ranade, A.N., Wankhede, S.S., Ranpise, N.S., Mundada, M.S., 2012. Development of bilayer floating tablet of amoxicillin and aloe vera gel powder for treatment of gastric ulcers. AAPS PharmSciTech. 13, 1518–1523. https://doi.org/10.1208/s12249-012-9882-4.
Ritger, P.L., Peppas, N.A., 1987a. A simple equation for description of solute release II. Fickian and anomalous release from swellable devices. J. Controll. Rel. 5, 37–42. https://doi.org/10.1016/0168-3659(87)90035-6.
Ritger, P.L., Peppas, N.A., 1987b. A simple equation for description of solute release I. Fickian and non-fickian release from non-swellable devices in the form of slabs, spheres, cylinders or discs. J. Controll. Rel. 5, 23–36. https://doi.org/10.1016/0168-3659(87)90034-4.
Rossi, A., Conti, C., Colombo, G., Castrati, L., Scarpignato, C., Barata, P., Sandri, G., Caramella, C., Bettini, R., Buttini, F., Colombo, P., 2016. Floating modular drug delivery systems with buoyancy independent of release mechanisms to sustain amoxicillin and clarithromycin intra-gastric concentrations. Drug Dev. Ind. Pharm. 42, 332–339. https://doi.org/10.3109/03639045.2015.1054397.
Sánchez-Cid, P., Romero, A., Díaz, M.J., De-Paz, M.V., Perez-Puyana, V., 2023. Chitosan-based hydrogels obtained via photoinitiated click polymer IPN reaction. J. Mol. Liq. 379, 1–11. https://doi.org/10.1016/j.molliq.2023.121735, 121735.
Scott, D.R., Sachs, G., Marcus, E.A., 2016. The role of acid inhibition in Helicobacter pylori eradication. F1000Res. 5, 1–7. https://doi.org/10.12688/F1000RESEARCH.8598.1.
Sharma, B., Sandilya, A., Patel, U., Shukla, A., Sadhu, S.D., 2021. A bio-inspired exploration of eco-friendly bael gum and guar gum-based bioadhesive as tackifiers for packaging applications. Int. J. Adhes. Adhesives 110, 102946. https://doi.org/10.1016/j.ijadhadh.2021.102946.
Siepmann, J., Peppas, N.A., 2012. Modeling of drug release from delivery systems based on hydroxypropyl methylcellulose (HPMC). Adv. Drug Deliv. Rev. 64, 163–174. https://doi.org/10.1016/j.addr.2012.09.028.
Singhvi, G., Singh, M., 2011. In-vitro drug release characterization models. Int. J. Pharm. Stud. Res. 2, 77–84.
American Cancer Society, Cancer Facts & Figures 2023, 2023. https://www.cancer.org/content/dam/cancer-org/research/cancer-facts-and-statistics/annual-cancer-facts-and-figures/2023/2023-cancer-facts-and-figures.pdf.
Sugano, K., 2018. Vonoprazan fumarate, a novel potassium-competitive acid blocker, in the management of gastroesophageal reflux disease: safety and clinical evidence to date. Ther. Adv. Vaccines. 11, 1–14. https://doi.org/10.1177/https.
Suzuki, S., Gotoda, T., Kusano, C., Ikehara, H., Ichijima, R., Ohyauchi, M., Ito, H., Kawamura, M., Ogata, Y., Ohtaka, M., Nakahara, M., Kawabe, K., 2020. Seven-day vonoprazan and low-dose amoxicillin dual therapy as first-line Helicobacter pylori treatment: a multicentre randomised trial in Japan. Gut 69, 1019–1026. https://doi.org/10.1136/gutjnl-2019-319954.
Tadros, M.I., 2010. Controlled-release effervescent floating matrix tablets of ciprofloxacin hydrochloride: development, optimization and in vitro–in vivo evaluation in healthy human volunteers. Eur. J. Pharm. Biopharm. 74, 332–339. https://doi.org/10.1016/j.ejpb.2009.11.010.
Thombre, N.A., Gide, P.S., 2016. Floating-bioadhesive gastroretentive Caesalpinia pulcherrima-based beads of amoxicillin trihydrate for Helicobacter pylori eradication. Drug Deliv. 23, 405–419. https://doi.org/10.3109/10717544.2014.916766.
Tripathi, G.K., Singh, S., Nath, G., 2012. Formulation and In-vitro evaluation of pH-sensitive oil entrapped polymeric blend amoxicillin beads for the eradication of Helicobacter pylori. Iran. J. Pharm. Res. 11, 447–455.
Tripathi, J., Thapa, P., Maharjan, R., Jeong, S.H., 2019. Current state and future perspectives on gastroretentive drug delivery systems. Pharmaceutics 11, 1–22. https://doi.org/10.3390/pharmaceutics11040193, 193.
Venkateswaramurthy, N., Sambathkumar, R., Perumal, P., 2011. Design and evaluation of controlled release mucoadhesive microspheres of amoxicillin for anti Helicobacter pylori therapy. Asian J. Pharm. 5, 238–245. https://doi.org/10.4103/0973-8398.97125.
Verdugo-Fernández, P.M., 2020. Stimuli Cleavable ABA Block copolymers: Synthesis of Degradable Thermoplastic Elastomers from Renewable Resources [dissertation]. Universitat Rovira i Virgili, Tarragona n.d.
Villegas, I., Rosillo, M.Á., Alarcón-de-la-Lastra, C., Vázquez-Román, V., Llorente, M., Sánchez, S., Gil, A.G., Alcalde, P., González, E., Rosell, E., Nieto, C., Fernandez-Campos, F., 2021. Amoxicillin and clarithromycin mucoadhesive delivery system for helicobacter pylori infection in a mouse model: characterization, pharmacokinetics, and efficacy. Pharmaceutics 13, 1–25. https://doi.org/10.3390/pharmaceutics13020153, 153.
Yang, J.C., Lu, C.W., Lin, C.J., 2014. Treatment of Helicobacter pylori infection: current status and future concepts. World J. Gastroenterol. 20, 5283–5293. https://doi.org/10.3748/wjg.v20.i18.5283.
Zhao, S., Lv, Y., Bin Zhang, J., Wang, B., Lv, G.J., Ma, X.J., 2014. Gastroretentive drug delivery systems for the treatment of Helicobacter pylori. World J. Gastroenterol. 20, 9321–9329. https://doi.org/10.3748/wjg.v20.i28.9321.